NASA MEMO 12-1-58L

NASA

MEMORANDUM

EFFECT OF TAIL DIHEDRAL ON LATERAL CONTROL EFFECTIVENESS AT HIGH SUBSONIC SPEEDS OF DIFFERENTIALLY DEFLECTED HORIZONTAL-TAIL SURFACES ON A CONFIGURATION HAVING A THIN HIGHLY TAPERED WING

By Paul G. Fournier

Langley Research Center
Langley Field, Va.

NATIONAL AERONAUTICS AND SPACE ADMINISTRATION

WASHINGTON

January 1959

Declassified April 12, 1961

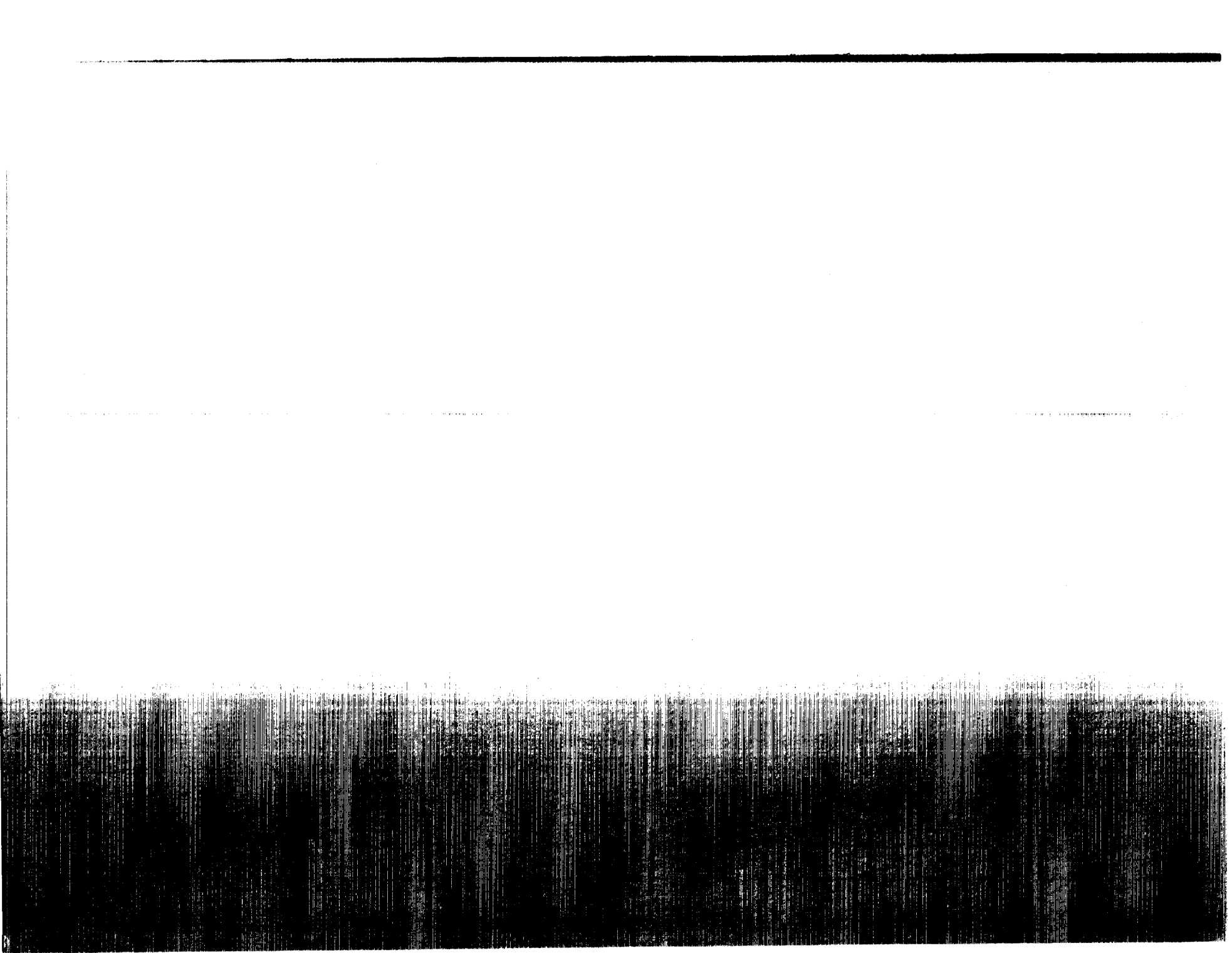

NATIONAL AERONAUTICS AND SPACE ADMINISTRATION

MEMORANDUM 12-1-58L

EFFECT OF TAIL DIHEDRAL ON LATERAL CONTROL EFFECTIVENESS AT HIGH SUBSONIC SPEEDS OF DIFFERENTIALLY DEFLECTED HORIZONTAL-TAIL SURFACES ON A CONFIGURATION HAVING A THIN HIGHLY TAPERED WING*

By Paul G. Fournier

SUMMARY

Tests have been conducted in the Langley high-speed 7- by 10-foot tunnel to determine the effect of tail dihedral on lateral control effectiveness of a complete-model configuration having differentially deflected horizontal-tail surfaces. Limited tests were made to determine the lateral characteristics as well as the longitudinal characteristics in sideslip. The wing had an aspect ratio of 3, a taper ratio of 0.14, 28.80° sweep of the quarter-chord line with zero sweep at the 80-percent-chord line, and NACA 65A004 airfoil sections. The test Mach number range extended from 0.60 to 0.92.

There are only small variations in the roll effectiveness parameter C_{l_δ} with negative tail dihedral angle. The tail size used on the test model, however, is perhaps inadequate for providing the roll rates specified by current military requirements at subsonic speeds. The lateral aerodynamic characteristics were essentially constant throughout the range of sideslip angle from 12° to -12°. A general increase in yawing moment was noted with increased negative dihedral throughout the Mach number range.

INTRODUCTION

The use of thin flexible wings for high-speed airplanes frequently has resulted in the loss of control effectiveness of conventional flap-type ailerons at high subsonic speeds which makes it necessary to

*Title, Unclassified.

consider other means of lateral control. A promising lateral control device presently being considered is an all-movable, differentially deflected horizontal tail. References 1 to 3 present lateral-control data for differentially deflected horizontal-tail surfaces for Mach numbers of 0.055 to 2.0. Data obtained prior to those presented in references 1 to 3 have been summarized in reference 4. These data include effects of wing plan form, aeroelasticity, and control deflection angle through wide ranges of angle of attack and angle of sideslip. Data have been obtained, however, only for constant dihedral angles, in most cases zero degree. Longitudinal stability requirements for high-speed airplanes have indicated the need for low horizontal-tail positions, which in some cases can only be accomplished by large negative tail dihedral angles.

This paper presents results of an investigation to determine the lateral control effectiveness as well as the stability characteristics of a differentially deflected horizontal tail through a systematic variation of dihedral angles from 0° to -30°. The results presented herein include only a very limited analysis.

SYMBOLS

The data are presented about the system of axes shown in figure 1. The moment coefficients are referred to a center-of-gravity location which is at the quarter-chord point of the wing mean aerodynamic chord.

C_D' drag coefficient (approximate), $\frac{\text{Drag}}{qS}$

C_L lift coefficient, $\frac{\text{Lift}}{qS}$

C_l rolling-moment coefficient, $\frac{\text{Rolling moment}}{qSb}$

$\Delta C_l, \Delta C_n, \Delta C_Y$ incremental forces and moments due to control deflection

$$C_{l_p} = \frac{\partial C_l}{\partial \frac{pb}{2V}}$$

$$C_{l_\delta} = \frac{\Delta C_l}{\delta}, \text{ per degree}$$

C_m pitching-moment coefficient, $\frac{\text{Pitching moment}}{qS\bar{c}}$

C_n yawing-moment coefficient, $\frac{\text{Yawing moment}}{qSb}$

$C_{n_\delta} = \frac{\Delta C_n}{\delta}$, per degree

$\frac{C_{n_\delta}}{C_{l_\delta}}$ ratio of yawing moment to rolling moment due to control deflection

C_Y lateral-force coefficient, $\frac{\text{Lateral force}}{qS}$

$C_{Y_\delta} = \frac{\Delta C_Y}{\delta}$, per degree

b wing span, ft

c local wing chord parallel to plane of symmetry, ft

$\bar{c}$ wing mean aerodynamic chord, $\frac{2}{S}\int_0^{b/2} c^2 dy$, ft

i_t effective angle of incidence of horizontal tail with respect to fuselage center line, deg

M Mach number

p rolling velocity, radians/sec

$\frac{pb}{2V}$ wing-tip helix angle, radians

q dynamic pressure, $\frac{\rho V^2}{2}$, lb/sq ft

S wing area, sq ft

V free-stream velocity, ft/sec

α angle of attack, deg

β angle of sideslip, deg

Γ dihedral angle of horizontal tail, deg

δ total roll-control deflection, $\delta_R - \delta_L$, deg

$\Lambda_{c/4}$ sweep angle of quarter-chord line, deg

ρ mass density of air, slugs/cu ft

Subscripts:

L left horizontal-tail panel

R right horizontal-tail panel

Model component designations:

F fuselage

H horizontal tail

V vertical tail

W wing

T.O. horizontal tail off

APPARATUS, MODEL, AND TESTS

Tests were conducted in the Langley high-speed 7- by 10-foot tunnel of a sting-supported model having a wing of aspect ratio 3, a taper ratio of 0.14, zero sweep at the 80-percent-chord line ($\Lambda_{c/4} = 28.80^\circ$), and NACA 65A004 airfoil sections parallel to the plane of symmetry. This wing is the same aspect-ratio-3 wing that was obtained by clipping the tips of a basic aspect-ratio-4 wing discussed in reference 5. The fuselage had a fineness ratio of 10.94 and was similar to the fuselage of reference 5 except for the cylindrical afterbody. The details of the fuselage are given in figure 2.

The model was so constructed that the horizontal-tail panel (mounted from the fuselage center line) could be individually deflected through an angle-of-incidence range from 15° to -15° in 5° increments and mounted to provide a dihedral-angle range from 30° to -30° from the wing-chord plane extended.

The horizontal and vertical tails had quarter-chord sweep angles of 14.37° and 28.00°, respectively, and unswept trailing edges. Details of the complete model are given in figure 2. A photograph of the model and support system is presented as figure 3 in which is shown the horizontal tail with asymmetric deflection.

The model was tested through a Mach number range from 0.60 to 0.92 with corresponding Reynolds numbers ranging from approximately 2.6×10^6 to 3.4×10^6, based on the wing mean aerodynamic chord. The angle-of-attack range varied with loading conditions, the maximum range being from about -2° to 22°.

Force tests were made to determine the effect of dihedral on the rolling effectiveness of an all-movable differentially deflected horizontal tail at dihedral angles of 0°, -15°, and -30°. Longitudinal and lateral aerodynamic characteristics were also obtained. The forces and moments were measured by means of a six-component electrical strain-gage balance mounted internally in the fuselage. Limited data were also obtained from tests through a range of sideslip angle from 12° to -12° at several constant angles of attack.

CORRECTIONS

Blockage corrections were applied to the data by the method of reference 6. Jet-boundary corrections to angle of attack and drag were applied in accordance with reference 7.

Tares due to the sting support have not been applied, except for a fuselage-base-pressure correction to drag, since from past experience it was found that these tares are negligible.

The angles of attack have been corrected for deflection of the sting support and balance under load. No attempt has been made to correct the data for aeroelastic distortion of the wing; however, such distortion is believed to be negligible since the wing was constructed of steel.

RESULTS

Lateral Characteristics

The lateral aerodynamic characteristics for the complete-model configuration are presented as increments of total control deflection in figures 4 to 11 for angles of dihedral of 0°, -15°, and -30°.

There are only small variations in the roll effectiveness parameter C_{l_δ} with negative tail dihedral angle at any given Mach number or angle of attack (at least up to $\alpha \approx 15^\circ$), as shown in figure 4 for constant total roll control deflection of -10° and in figure 9 for constant effective tail incidence. The dashed curves in figure 4 represent the values of C_{l_δ} at the trim angle of attack with the center of gravity at $\bar{c}/4$ for various effective stabilizer angles. These results are summarized in figure 5.

In order to provide an approximate assessment of the adequacy of the present lateral-control system, simple one-degree-of-freedom calculations were made to determine the rolling-moment coefficient required in order to satisfy current flying qualities requirements. Experimental values of the damping-in-roll derivative C_{l_p} were obtained from reference 8 for an aspect-ratio-3 wing. A value of $\frac{pb}{2V} = 0.09$ was used, since reference 9 specifies this value within the range from 1.1 times stalling speed to minimum combat speed for fighter-type aircraft. The resulting required value of ΔC_l is approximately 0.025, which is about 30 percent more than was achieved with a total differential tail deflection of 30°. These calculations, of course, are very approximate; however, it would seem that the tail size used on the present model is smaller than should be provided to meet current subsonic roll requirements for fighter-type aircraft.

There was a general increase in C_{n_δ} with increasing negative dihedral throughout the Mach number range and for angles of attack up to at least 15° for conditions of either constant control deflection or of constant effective stabilizer angle, as may be seen in figures 6 and 10. There was a corresponding variation in the lateral force increment C_{Y_δ}. (See figs. 7 and 11.) These effects are due to increases in the lateral component of the horizontal-tail loads which increased with negative dihedral. Figure 8 presents the ratio of the yawing moment to rolling moment due to control deflection $\frac{C_{n_\delta}}{C_{l_\delta}}$ for the configurations having constant control deflection. These data indicate that the yawing moment increases substantially with increasing negative dihedral angle throughout the Mach number range. The configuration having $i_t = -10^\circ$ showed wide variations with angle of attack particularly at $M = 0.90$ and 0.92. These variations were due principally to the low values of C_{l_δ} in this Mach number range shown in figure 4(b) rather than to the variation in C_{n_δ}.

The effect of the vertical tail on the incremental lateral characteristics is shown in figure 12 for $M = 0.80$ and $\delta = -20^\circ$ $(i_t = 0^\circ)$ for each value of dihedral angle Γ. The vertical tail tends to decrease the rolling moment throughout the range of angle of attack (fig. 12(a)). This effect on C_{l_δ} is in the direction expected for the loads induced on the vertical tail by asymmetrical deflection of the horizontal tail. Increases in negative dihedral angle (in effect lowering the horizontal tail) decreased the induced loads carried by the vertical tail by as much as 40 percent, as may be seen in figures 12(b) and 12(c).

The lateral aerodynamic characteristics due to differential deflection of the horizontal tail with and without the vertical tail, shown in figure 13 for a representative value of M of 0.80 at $\alpha = 0^\circ$, were essentially constant through the range of sideslip angles.

Longitudinal Characteristics

The longitudinal characteristics of the complete-model configuration with both symmetrical and asymmetrical deflection of the horizontal tail for the range of dihedral angles investigated, along with tail-off characteristics, are presented in figures 14 to 16. (In order to facilitate presentation of the data, staggered scales have been used in several of the figures and care should be taken in identifying the proper scale for each curve.)

The overall trends of the pitching-moment characteristics above 10° angle of attack for a given dihedral angle are generally similar for either the symmetrical or asymmetrical (roll control) deflection at a given effective stabilizer setting. Increasing the negative dihedral of the horizontal tail improved the linearity of the pitching-moment curves up to $\alpha \approx 15^\circ$ as would be expected (see figs. 14(c), 15(c), and 16(c)) for this type of configuration. Figure 17 shows that the variations of C_L, C_D', and C_m with sideslip angle are not greatly affected by tail dihedral.

CONCLUSIONS

From tests conducted in the Langley high-speed 7- by 10-foot tunnel of differentially deflected horizontal-tail surfaces on a configuration having a low-aspect-ratio thin wing through a range of negative tail dihedral angles, the following conclusions can be made:

1. There are only small variations in the roll effectiveness parameter C_{l_δ} with negative tail dihedral angle. The tail size used on the test model, however, is perhaps inadequate for providing the roll rates specified by current military requirements at subsonic speeds.

2. There was a general increase in yawing moment with increase in negative dihedral throughout the Mach number range up to an angle of attack of 15°.

3. The lateral aerodynamic characteristics were essentially constant throughout the range of sideslip angle from 12° to -12° at a Mach number of 0.80.

Langley Research Center,
National Aeronautics and Space Administration,
Langley Field, Va., October 1, 1958.

REFERENCES

1. Mitchell, Jesse L., and Vitale, A. James: Free-Flight Investigation of the Control Effectiveness of a Differentially Deflected Horizontal Tail at Mach Numbers From 0.8 to 1.6. NACA RM L56B20, 1956.

2. Boisseau, Peter C.: Low-Speed Roll Effectiveness of a Differentially Deflected Horizontal-Tail Surface on a 42° Swept-Wing Model. NACA RM L56E03, 1956.

3. Spearman, M. Leroy: Limited Investigation of Effects of Differential Horizontal-Tail Deflection on Lateral Control Characteristics of Two Swept-Wing Airplane Models at Mach Numbers From 1.4 to 2.0. NACA RM L56I20, 1956.

4. Campbell, John P.: The Use of the Horizontal Tail for Roll Control. NACA RM L55L16a, 1956.

5. Goodson, Kenneth W.: Static Longitudinal Characteristics at High Subsonic Speeds of a Complete Airplane Model With a Highly Tapered Wing Having the 0.80 Chord Line Unswept and With Several Tail Configurations. NACA RM L56J03, 1957.

6. Herriot, John G.: Blockage Corrections for Three-Dimensional-Flow Closed-Throat Wind Tunnels, With Consideration of the Effect of Compressibility. NACA Rep. 995, 1950. (Supersedes NACA RM A7B28.)

7. Gillis, Clarence L., Polhamus, Edward C., and Gray, Joseph L., Jr.: Charts for Determining Jet-Boundary Corrections for Complete Models in 7- by 10-Foot Closed Rectangular Wind Tunnels. NACA WR L-123, 1945. (Formerly NACA ARR L5G31.)

8. Sleeman, William C., Jr., and Few, Albert G., Jr.: Experimental Investigation at High Subsonic Speed of the Rolling Stability Derivatives of a Complete Model Having a Clipped-Delta Wing and a High Horizontal Tail. NACA RM L55K11, 1956.

9. Anon.: Flying Qualities of Piloted Airplanes. Military Specification MIL-F-8785(ASG), Sept. 1, 1954; Amendment-1, Oct. 19, 1954.

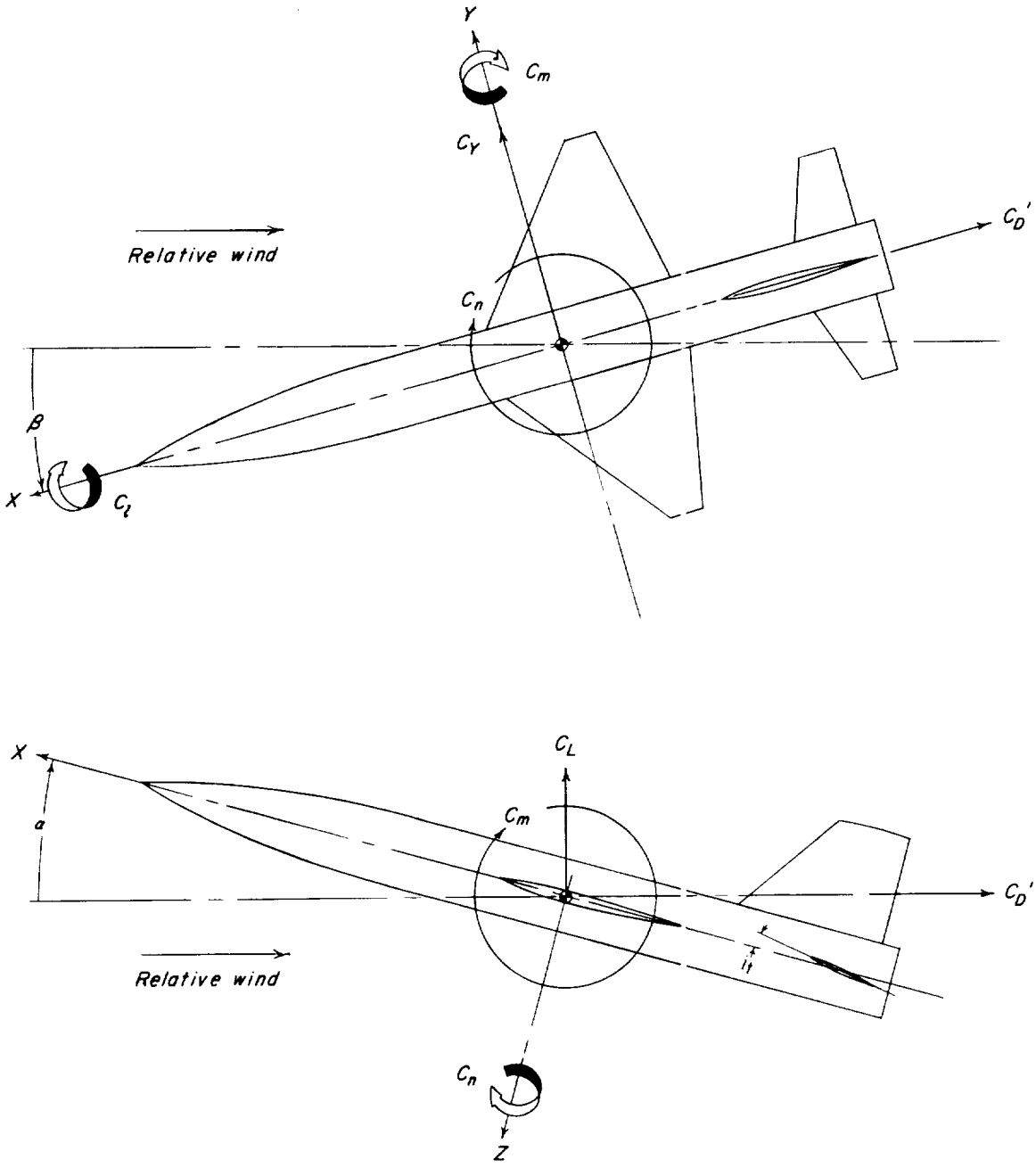

Figure 1.- Axes system and convention used to define positive sense of forces, moments, and angles.

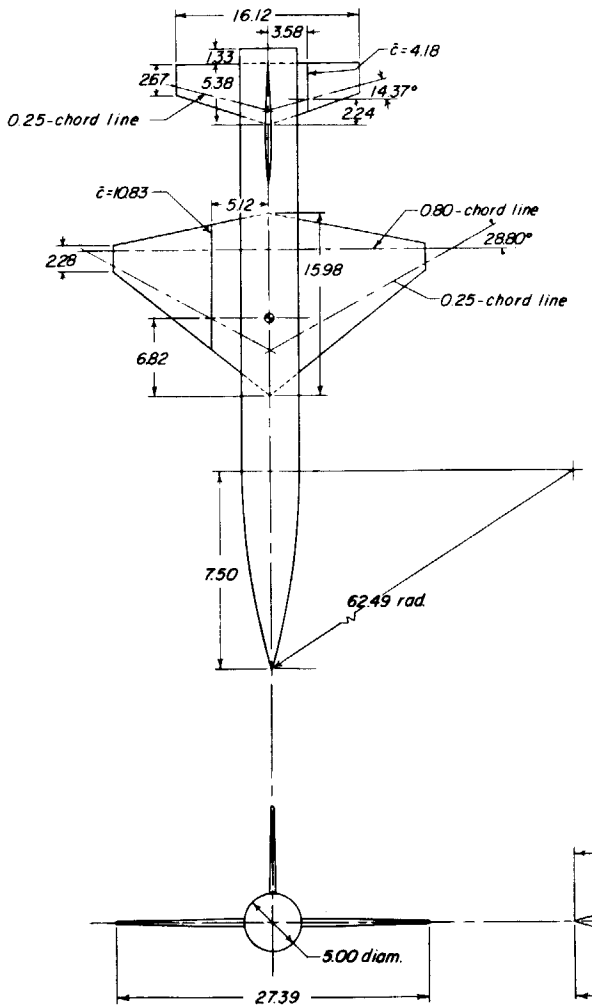

Geometric Characteristics

Wing:	
Sweep of $c/4$, deg	28.80
Area, sq ft	1.74
Span, ft	2.28
Aspect ratio	3
Taper ratio	.14
Mean aerodynamic chord, ft	.90
Airfoil section parallel to plane of symmetry	NACA 65A004
Horizontal tail:	
Sweep of $c/4$, deg	14.37
Area, sq ft	.45
Aspect ratio	4
Airfoil section parallel to plane of symmetry	NACA 65A006
Vertical tail:	
Sweep of $c/4$, deg	28.00
Area, sq ft	.60
Aspect ratio	1.16
Airfoil section parallel to plane of symmetry	NACA 65A006

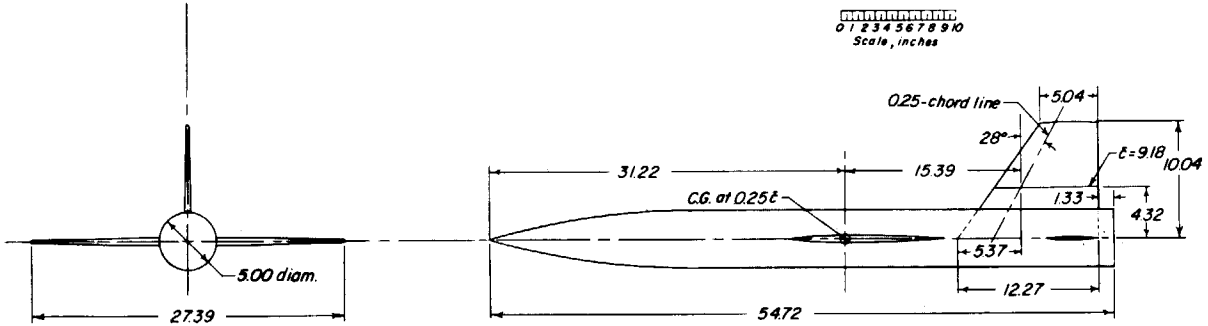

Figure 2.- Details of model. (All dimensions are in inches unless otherwise indicated.)

Figure 3.- Model mounted in tunnel. L-93205

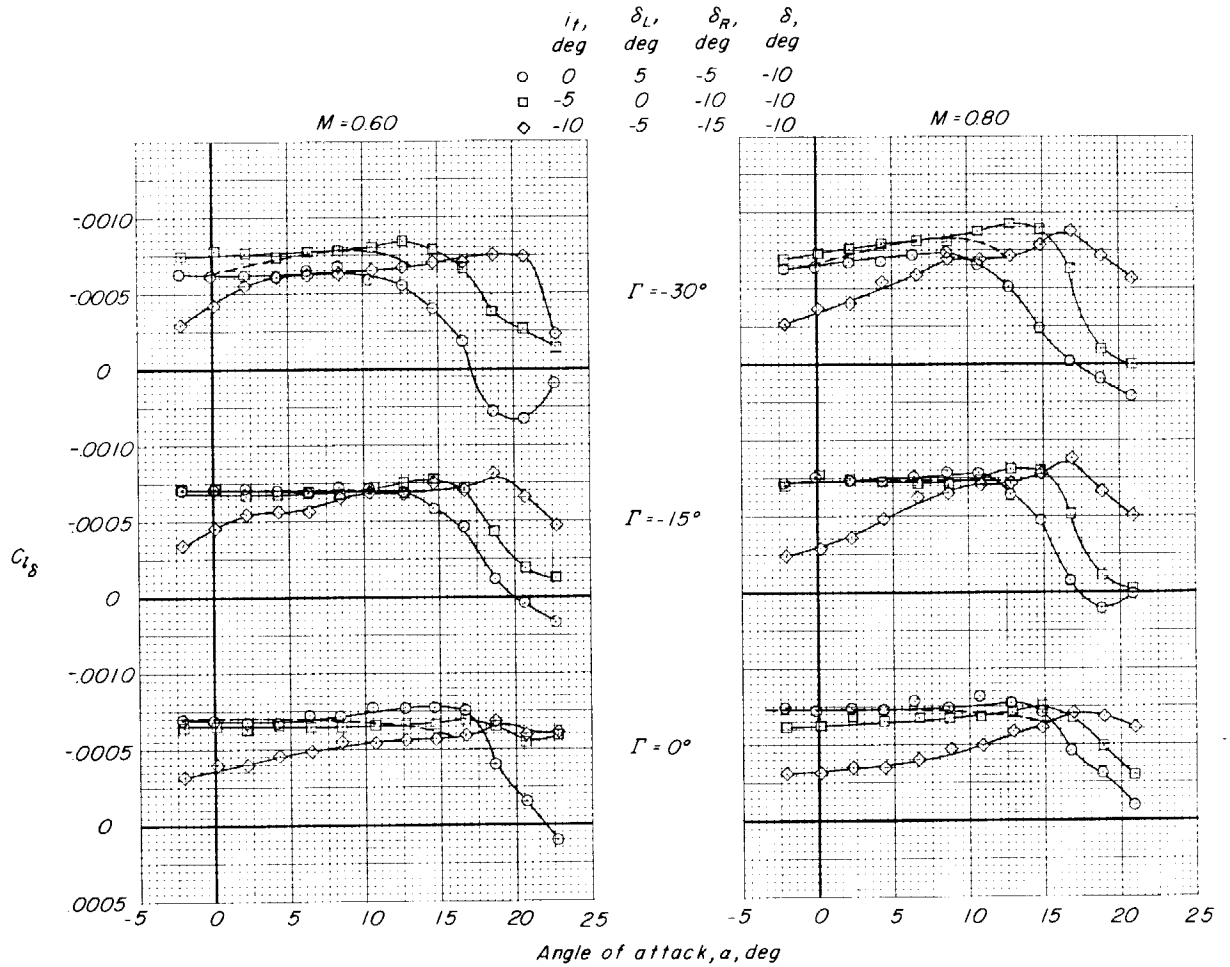

(a) M = 0.60 and 0.80.

Figure 4.- Variation with angle of attack of the roll-control parameter for each tail dihedral angle and a constant control deflection through a range of effective stabilizer settings. Center-of-gravity location at $\bar{c}/4$.

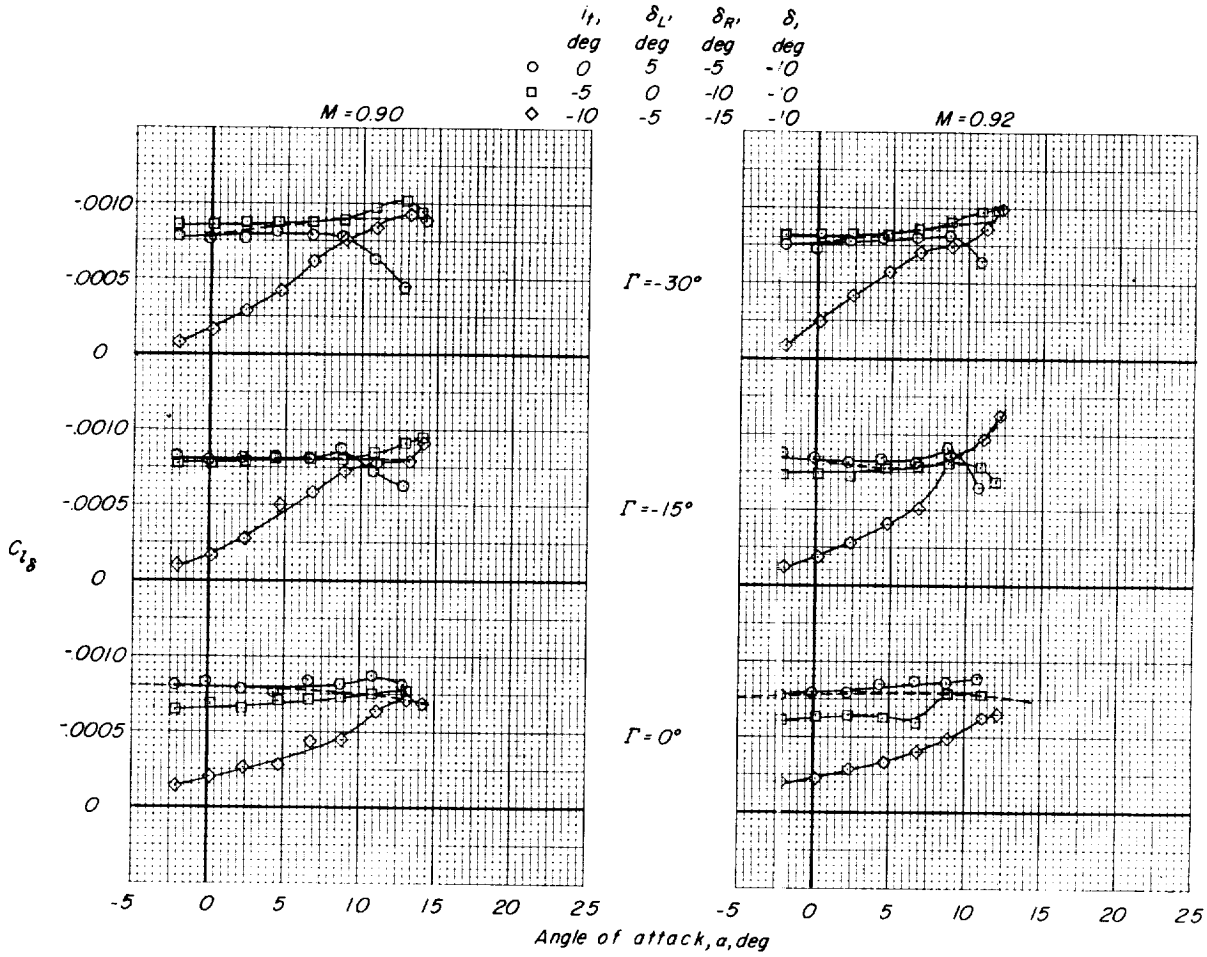

(b) M = 0.90 and 0.92.

Figure 4.- Concluded.

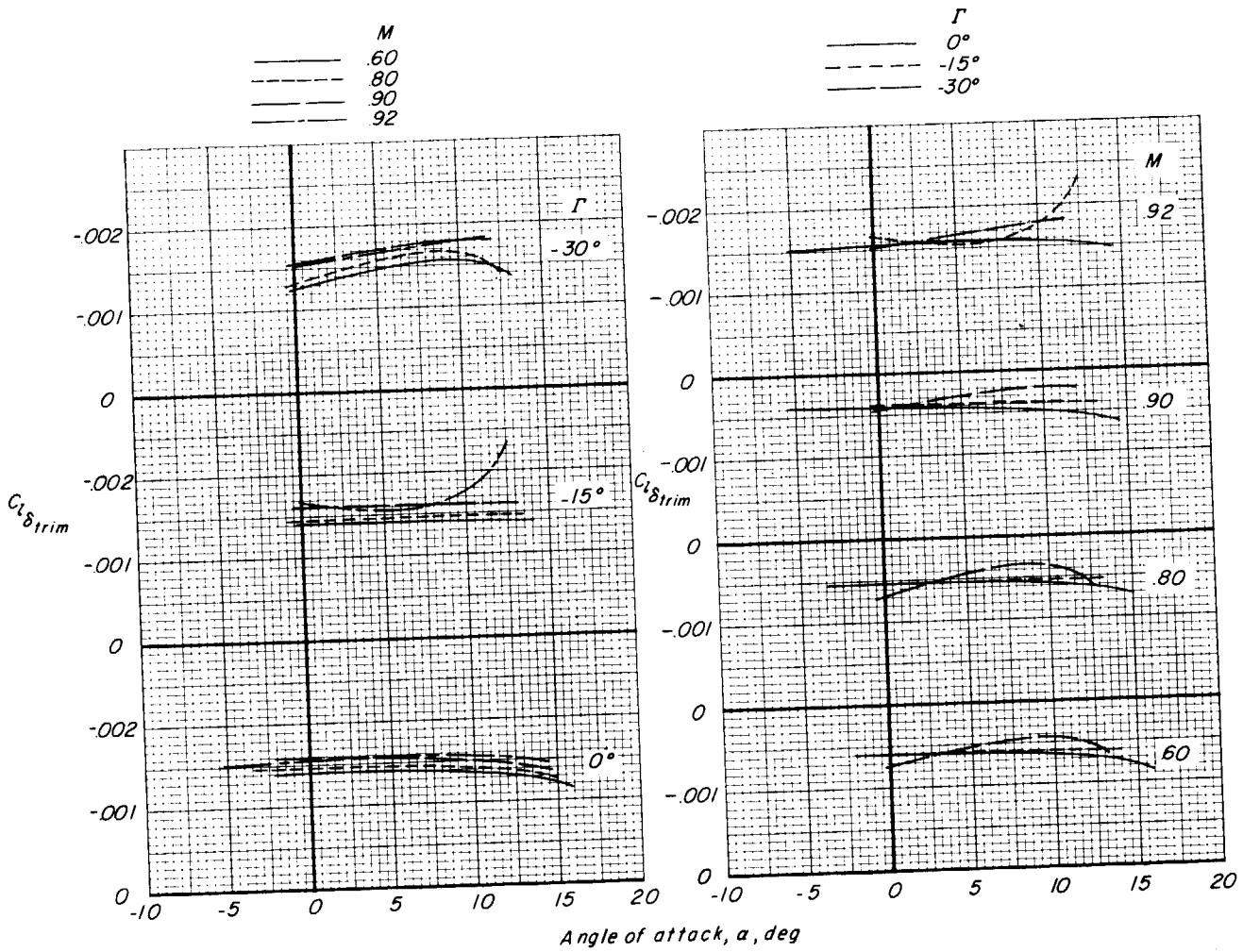

Figure 5.- Variation with angle of attack of $C_{l_{\delta_{trim}}}$ for a constant control deflection of -10° for each dihedral angle. Center-of-gravity location at $\bar{c}/4$.

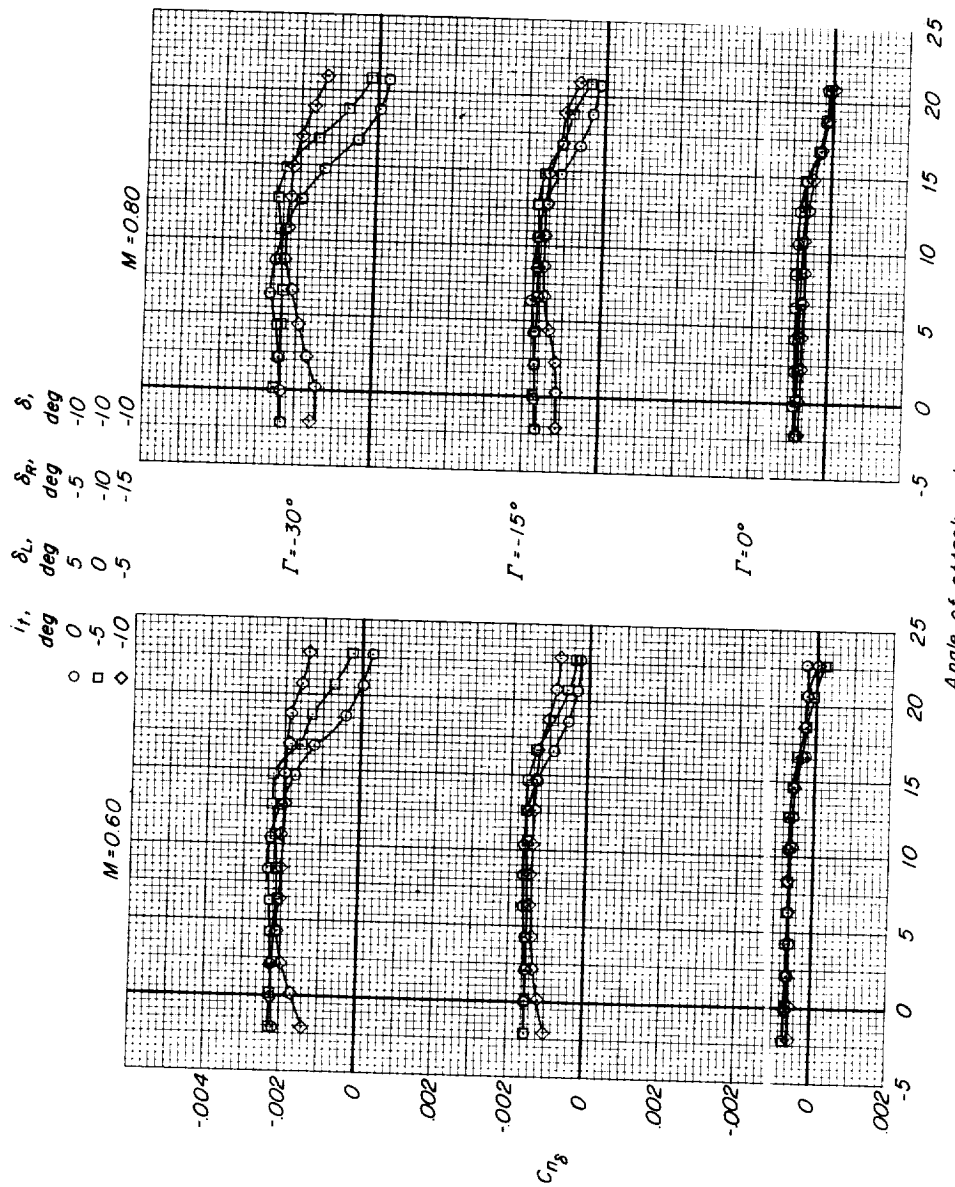

(a) M = 0.60 and 0.80.

Figure 6.- Variation with angle of attack of the yawing-moment parameter for each tail dihedral angle and a constant control deflection through a range of effective stabilizer settings. Center-of-gravity location at $\bar{c}/4$.

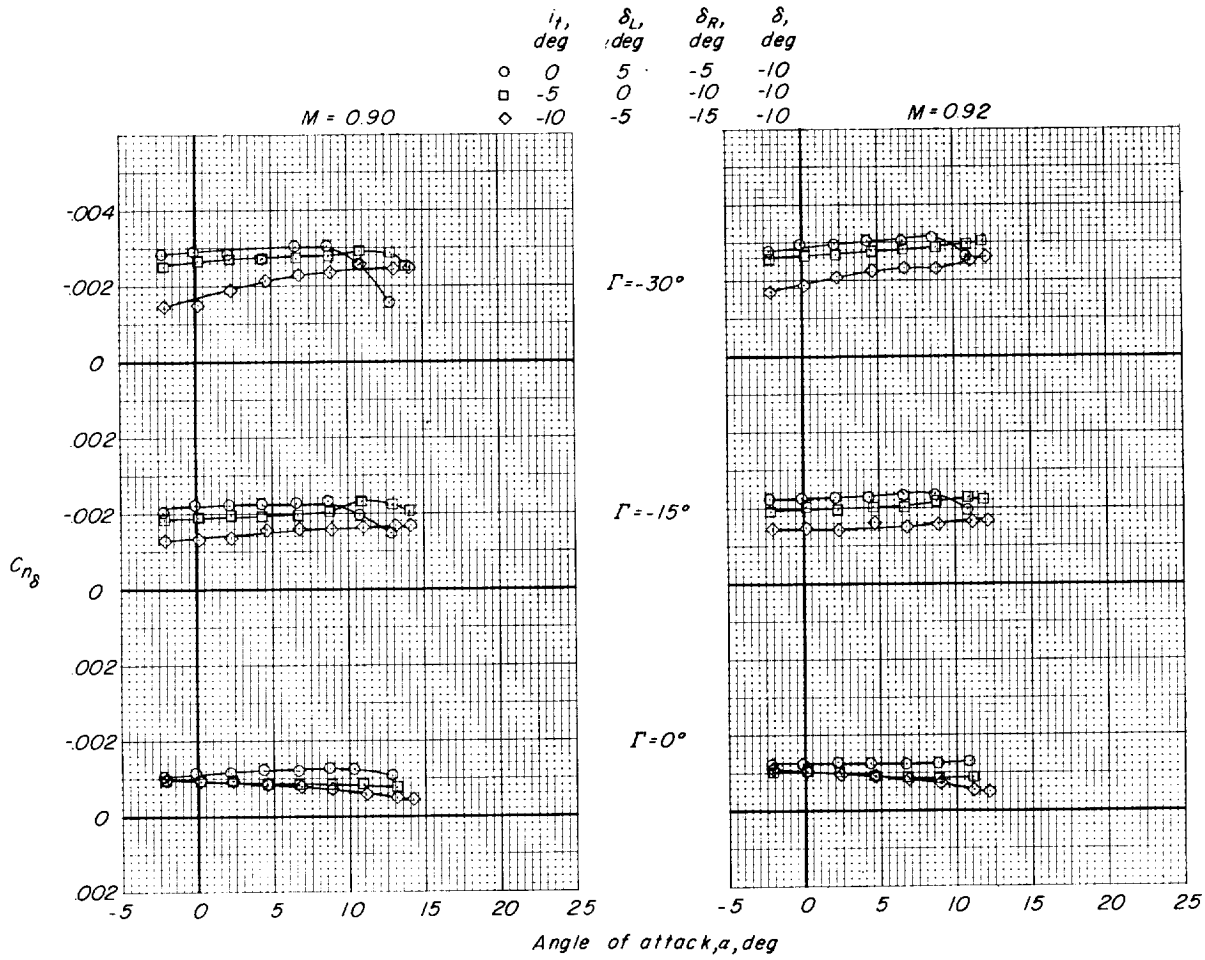

(b) M = 0.90 and 0.92.

Figure 6.- Concluded.

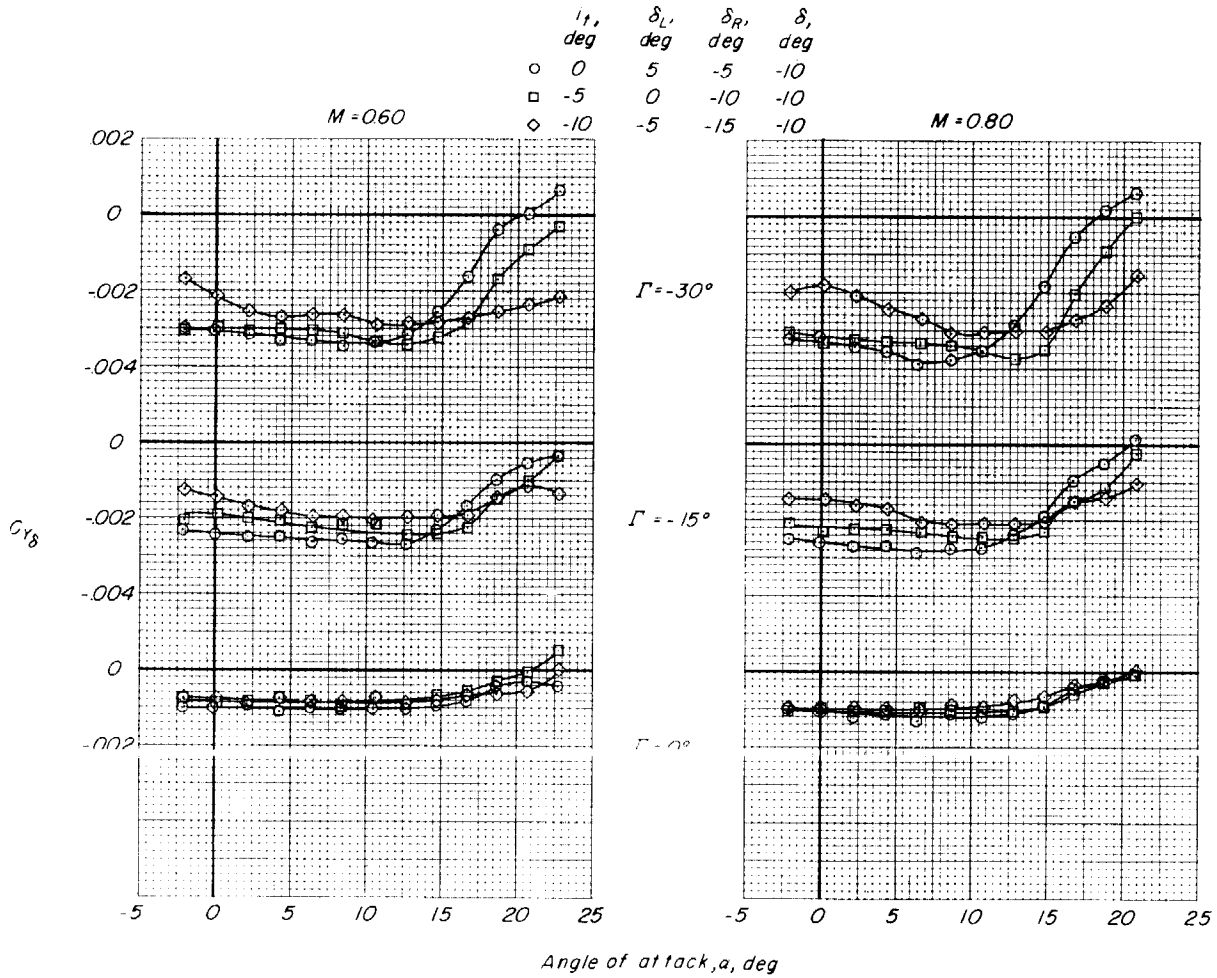

(a) M = 0.60 and 0.80.

Figure 7.- Variation with angle of attack of the lateral-force parameter for each tail dihedral angle and a constant control deflection through a range of effective stabilizer settings. Center-of-gravity location at $\bar{c}/4$.

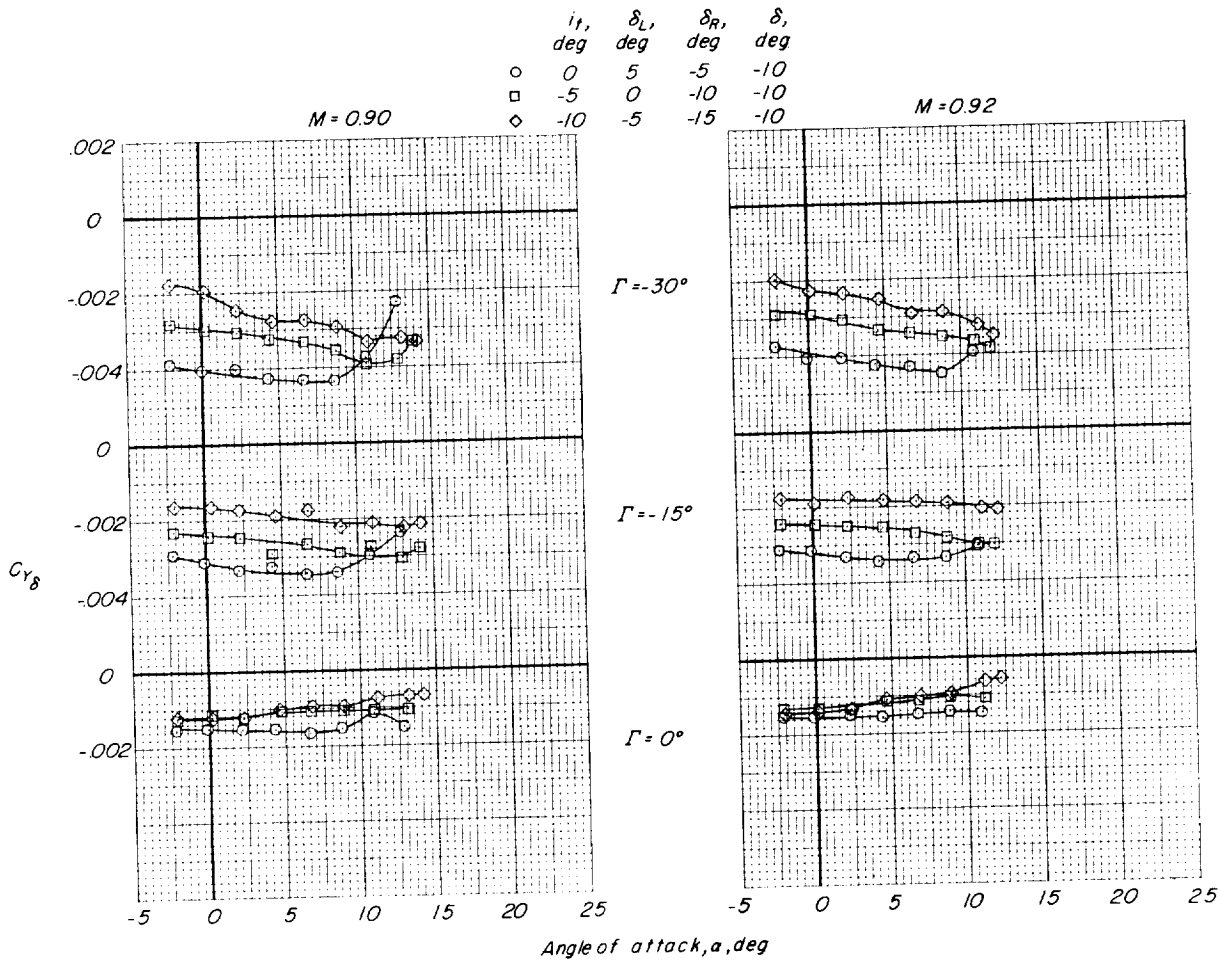

(b) M = 0.90 and 0.92.

Figure 7.- Concluded.

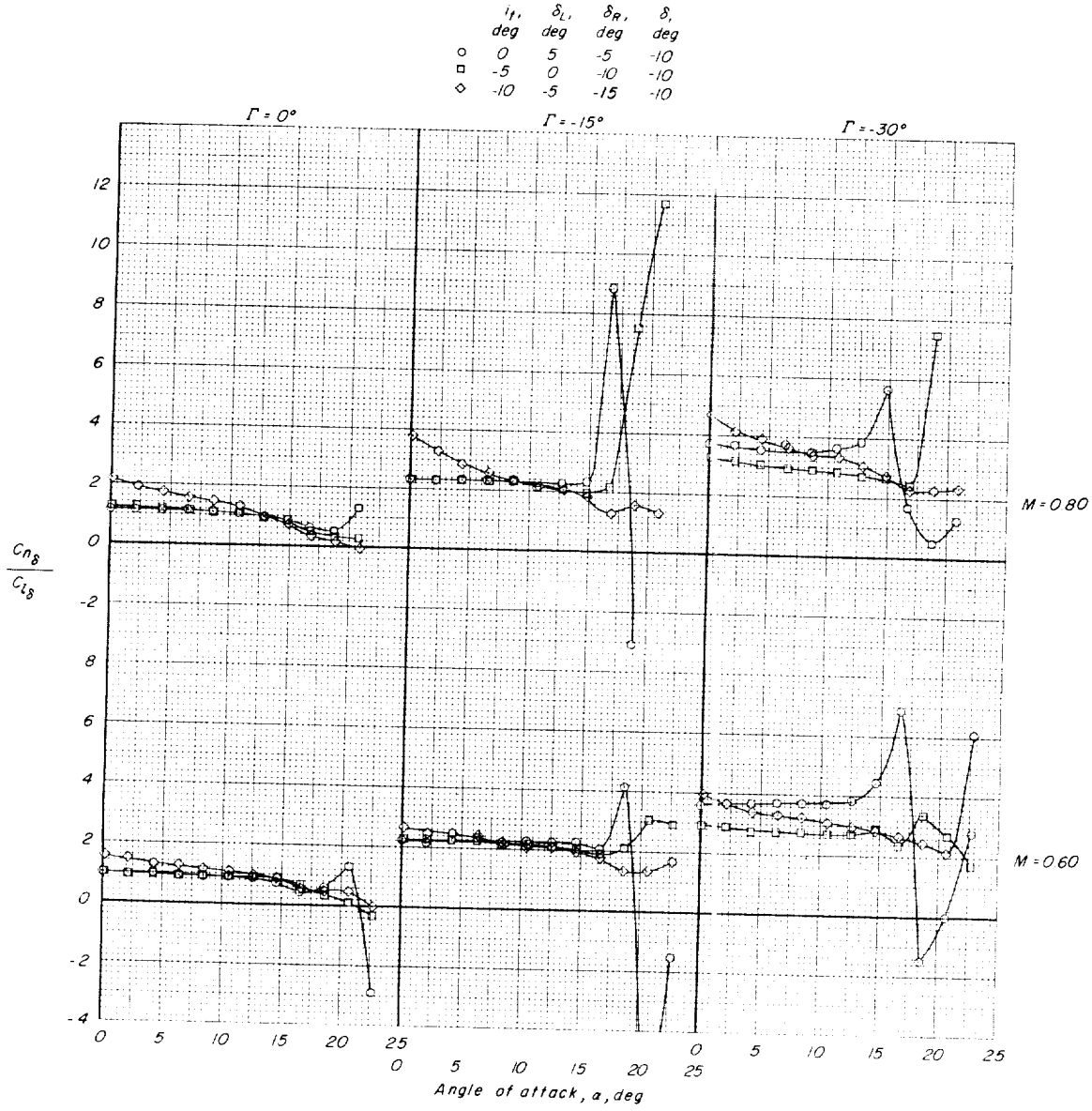

(a) M = 0.60 and 0.80.

Figure 8.- Variation with angle of attack of the ratio of yawing-moment parameter to roll-control parameter for each tail dihedral angle and a constant control deflection through a range of effective stabilizer settings.

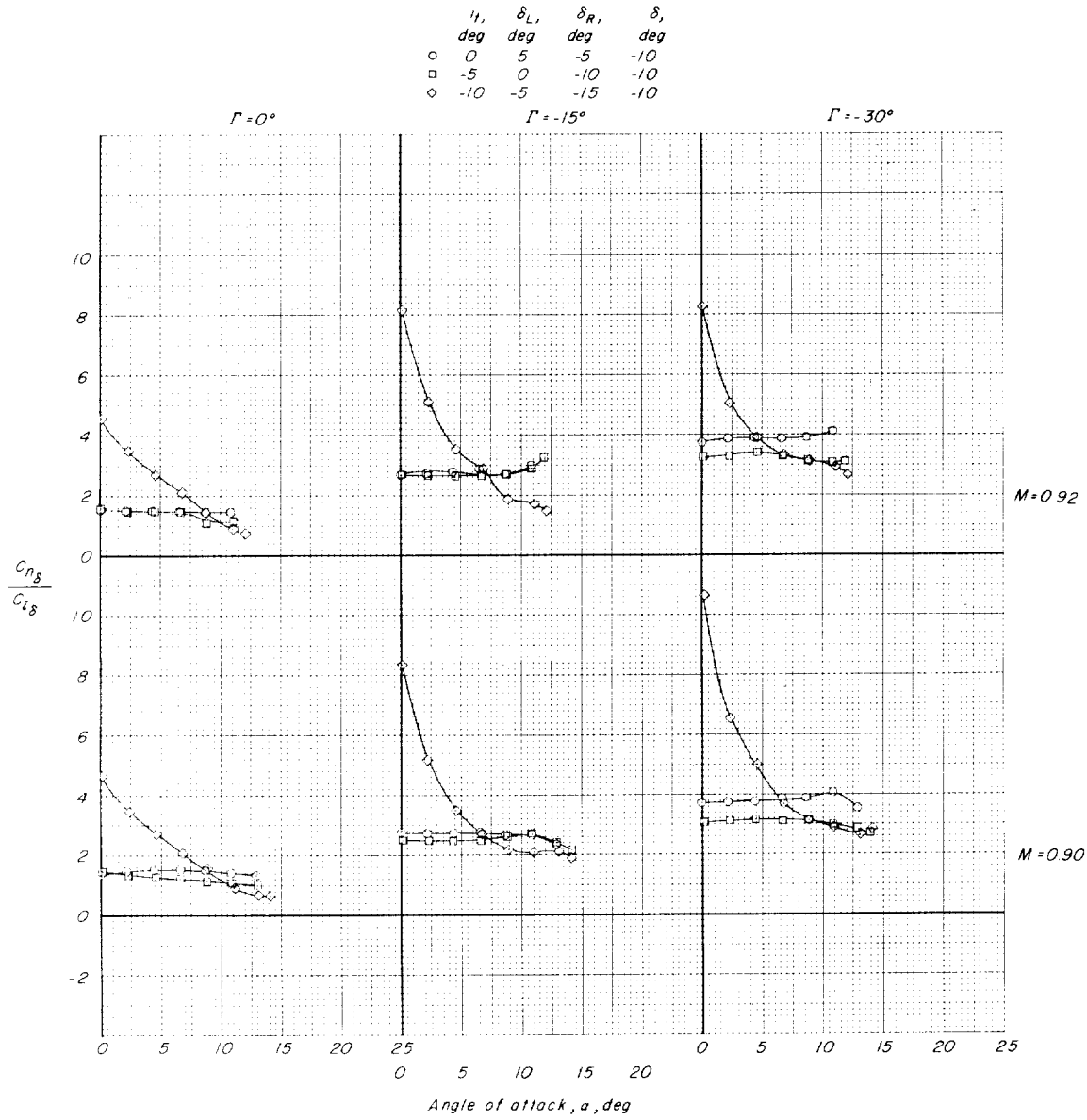

(b) M = 0.90 and 0.92.

Figure 8.- Concluded.

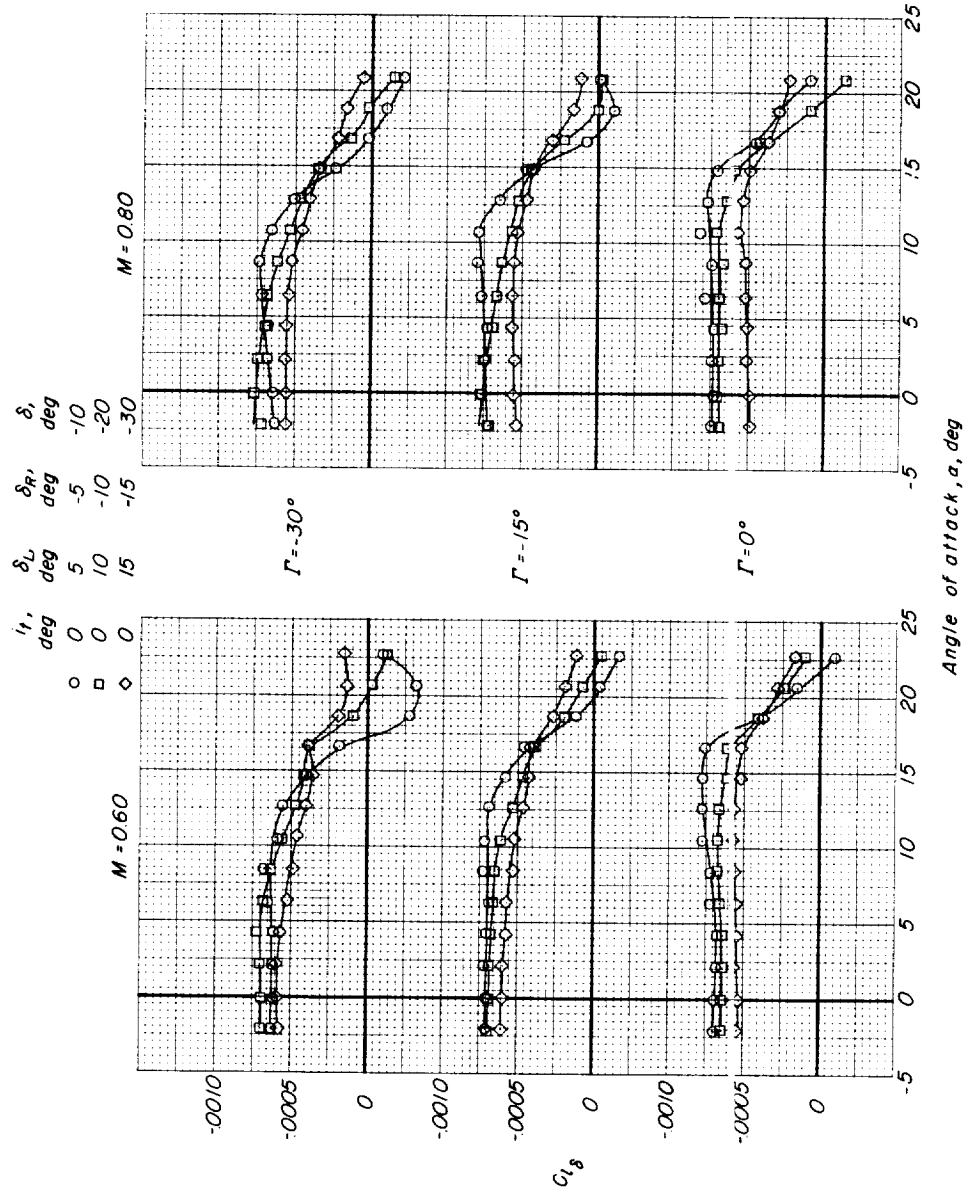

(a) M = 0.60 and 0.80.

Figure 9.- Variation with angle of attack of the roll-control parameter for each tail dihedral angle and a constant effective stabilizer setting through a range of control deflections.

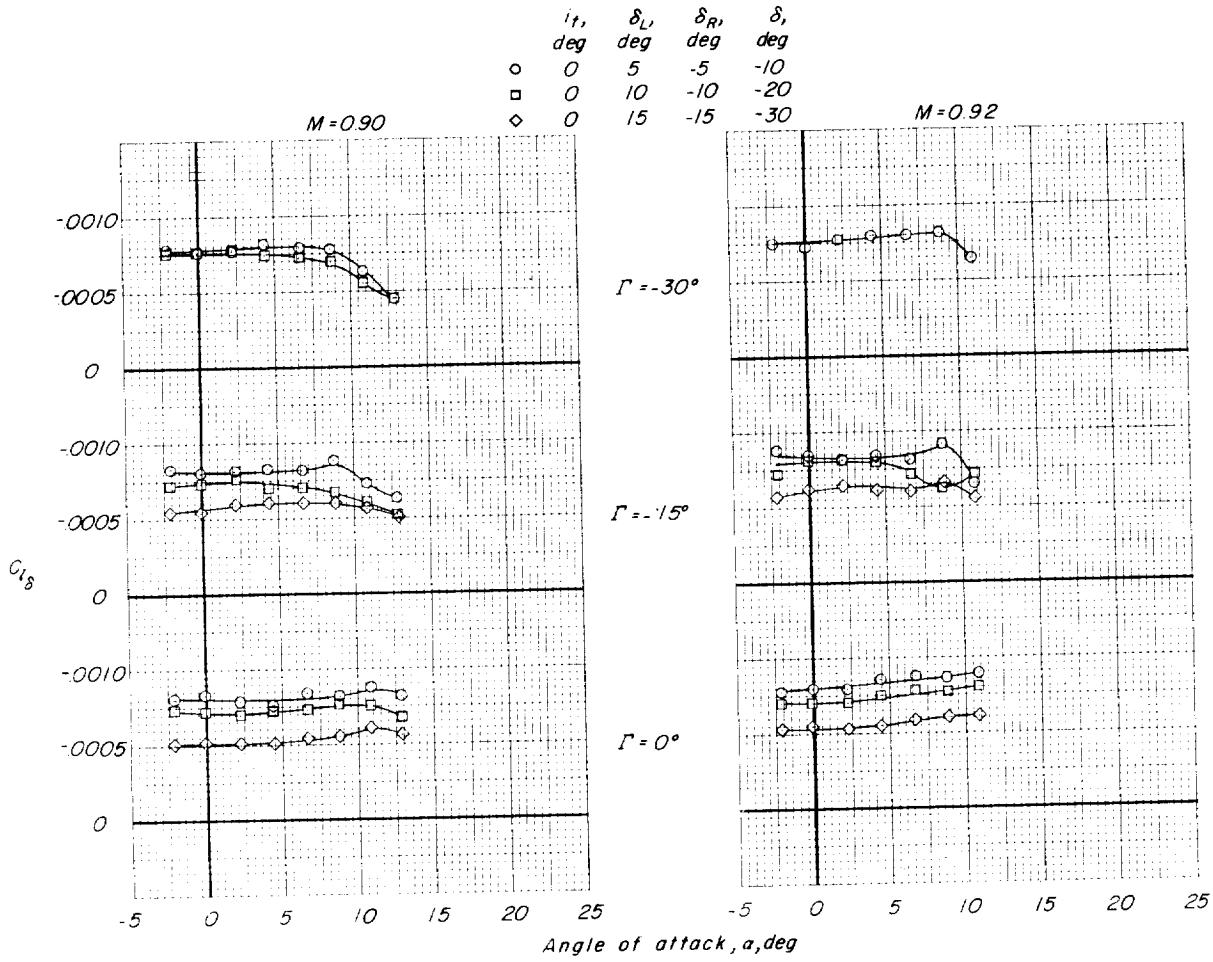

(b) M = 0.90 and 0.92.

Figure 9.- Concluded.

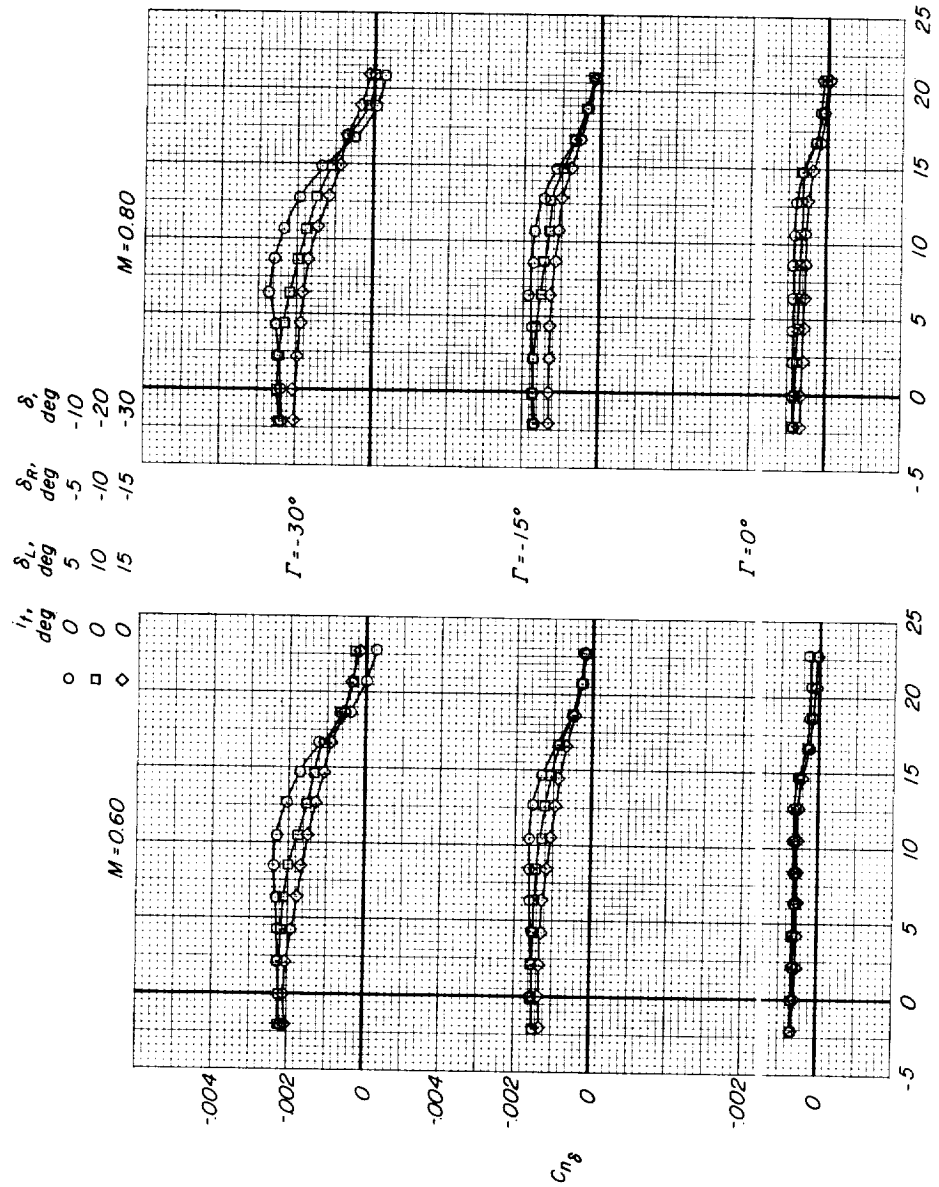

(a) M = 0.60 and 0.80.

Figure 10.- Variation with angle of attack of the yawing-moment parameter for each tail dihedral angle and a constant effective stabilizer setting through a range of control deflections.

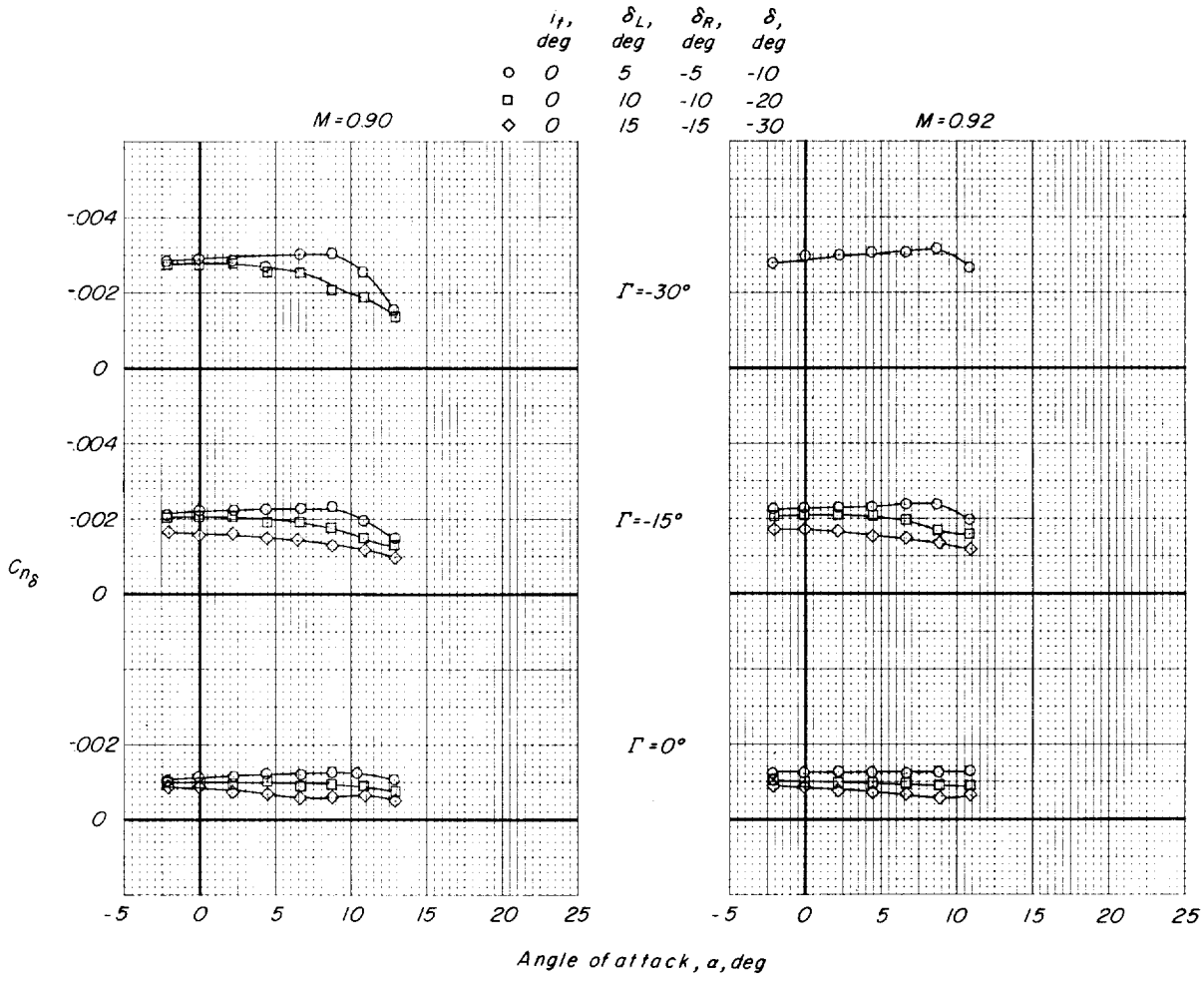

(b) M = 0.90 and 0.92.

Figure 10.- Concluded.

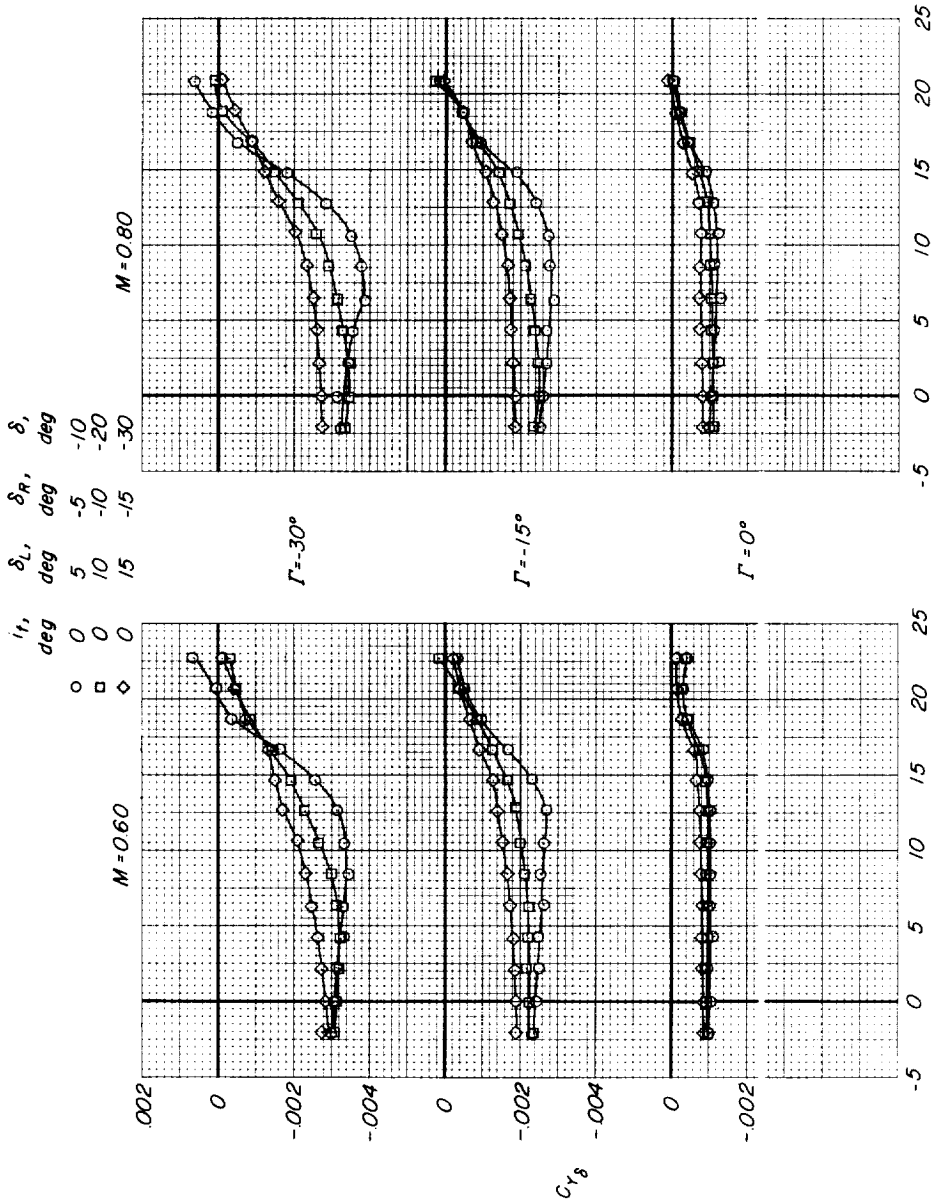

(a) M = 0.60 and 0.80.

Figure 11.- Variation with angle of attack of the lateral-force parameter for each tail dihedral angle and a constant effective stabilizer setting through a range of control deflections.

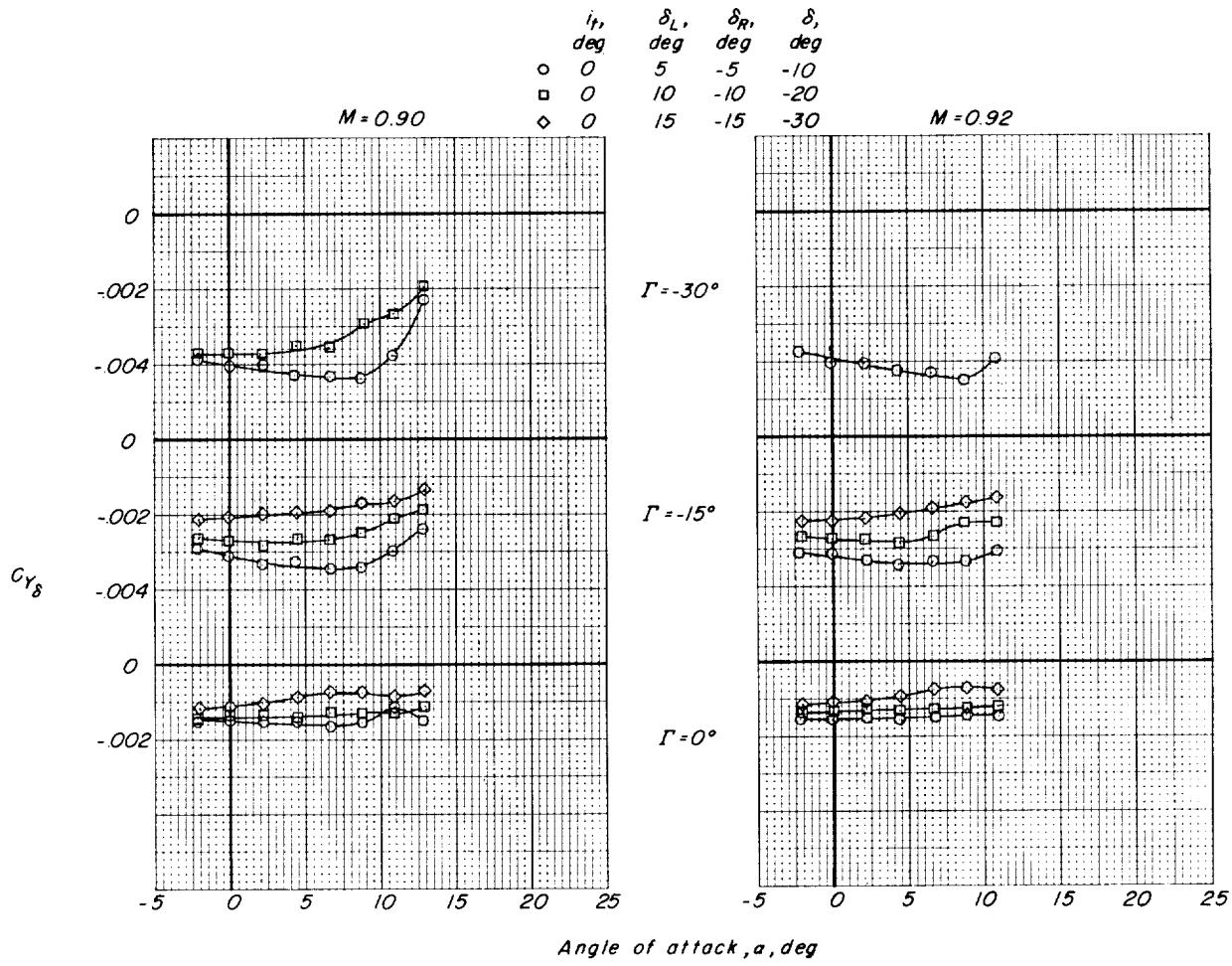

(b) M = 0.90 and 0.92.

Figure 11.- Concluded.

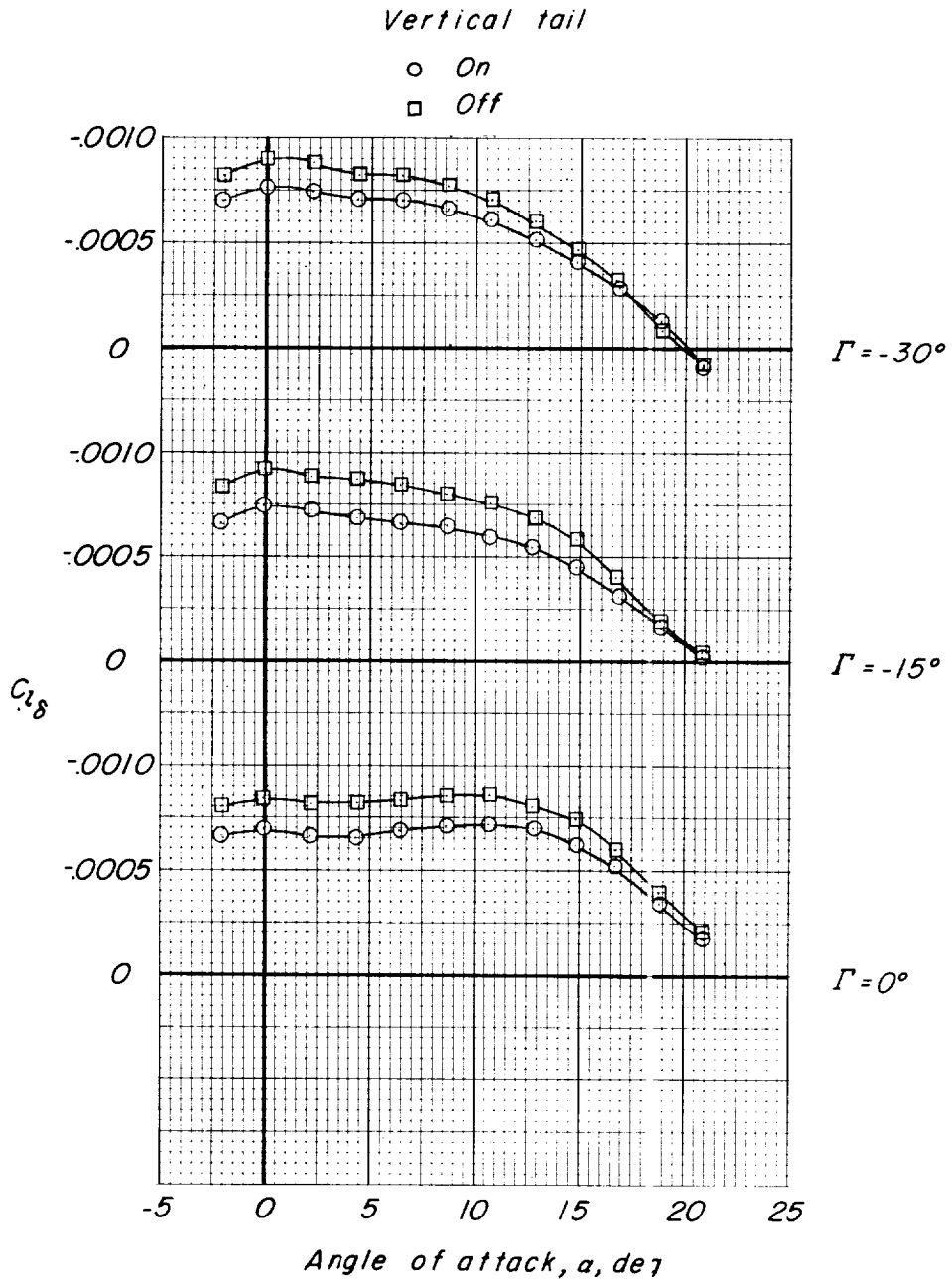

(a) Variation of C_{l_δ} with α.

Figure 12.- Variation with angle of attack of the effect of the vertical tail on the lateral characteristics for a control deflection of -20° and each tail dihedral angle at M = 0.80.

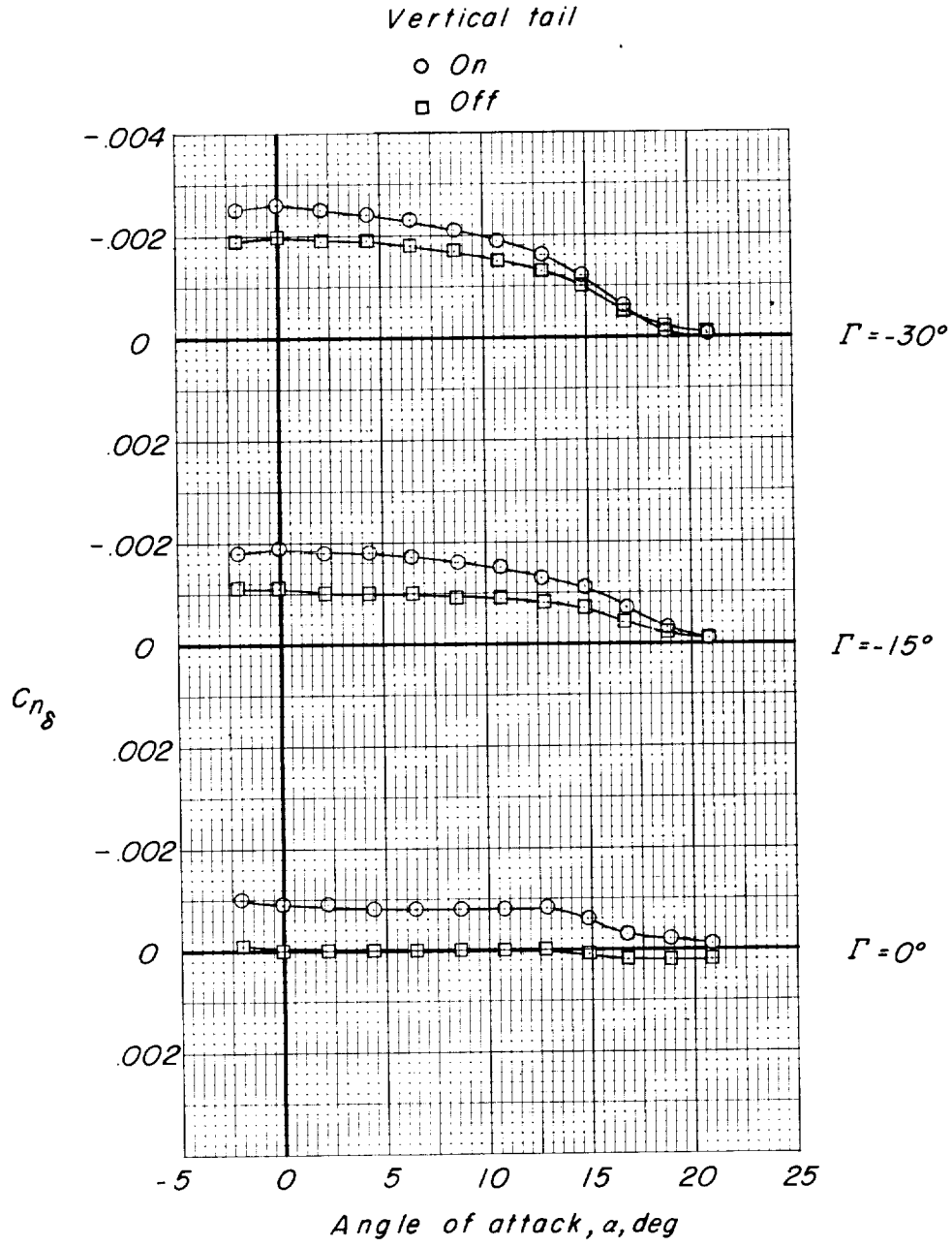

(b) Variation of C_{n_δ} with α.

Figure 12.- Continued.

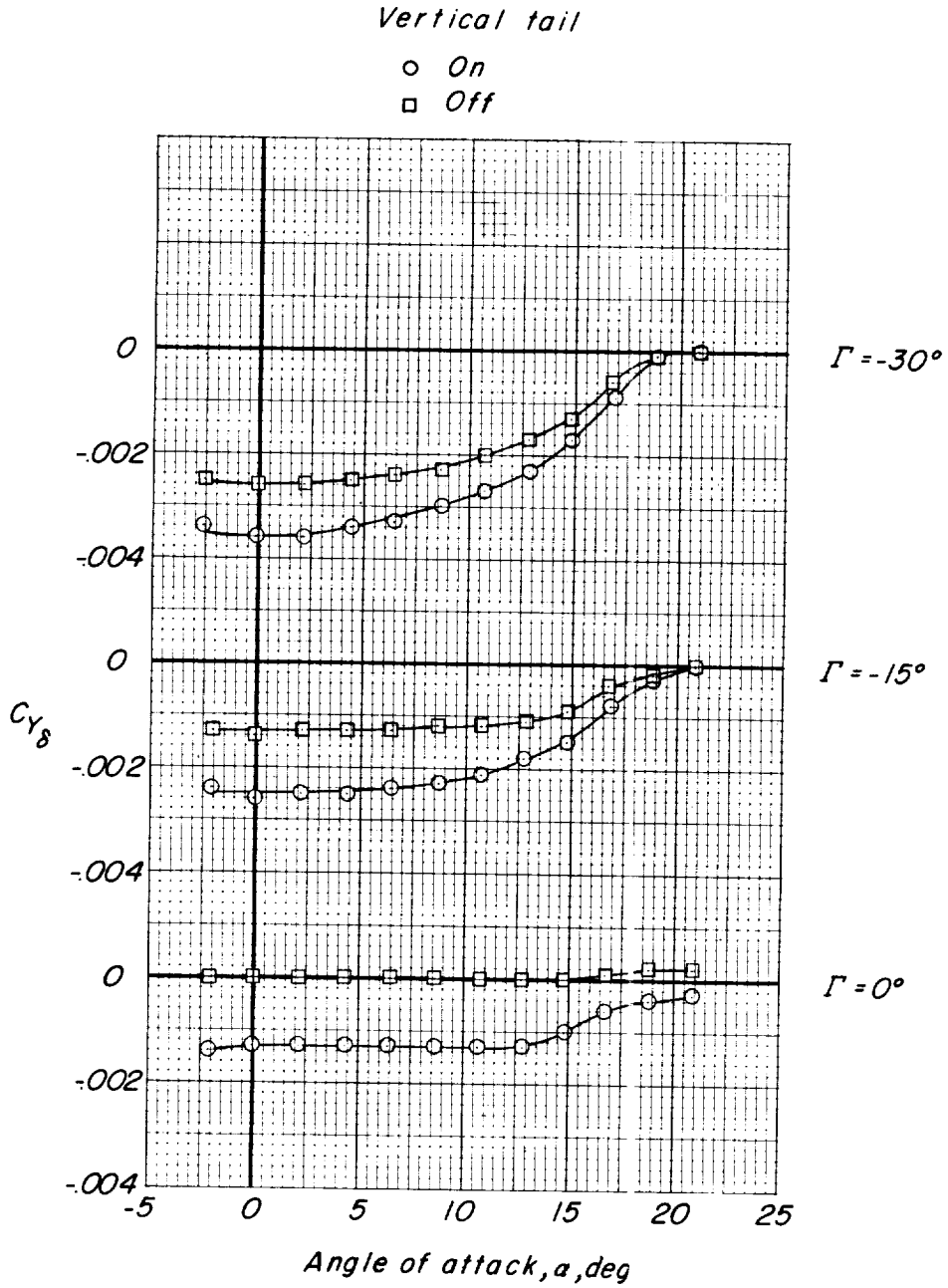

(c) Variation of C_{Y_δ} with α.

Figure 12.- Concluded.

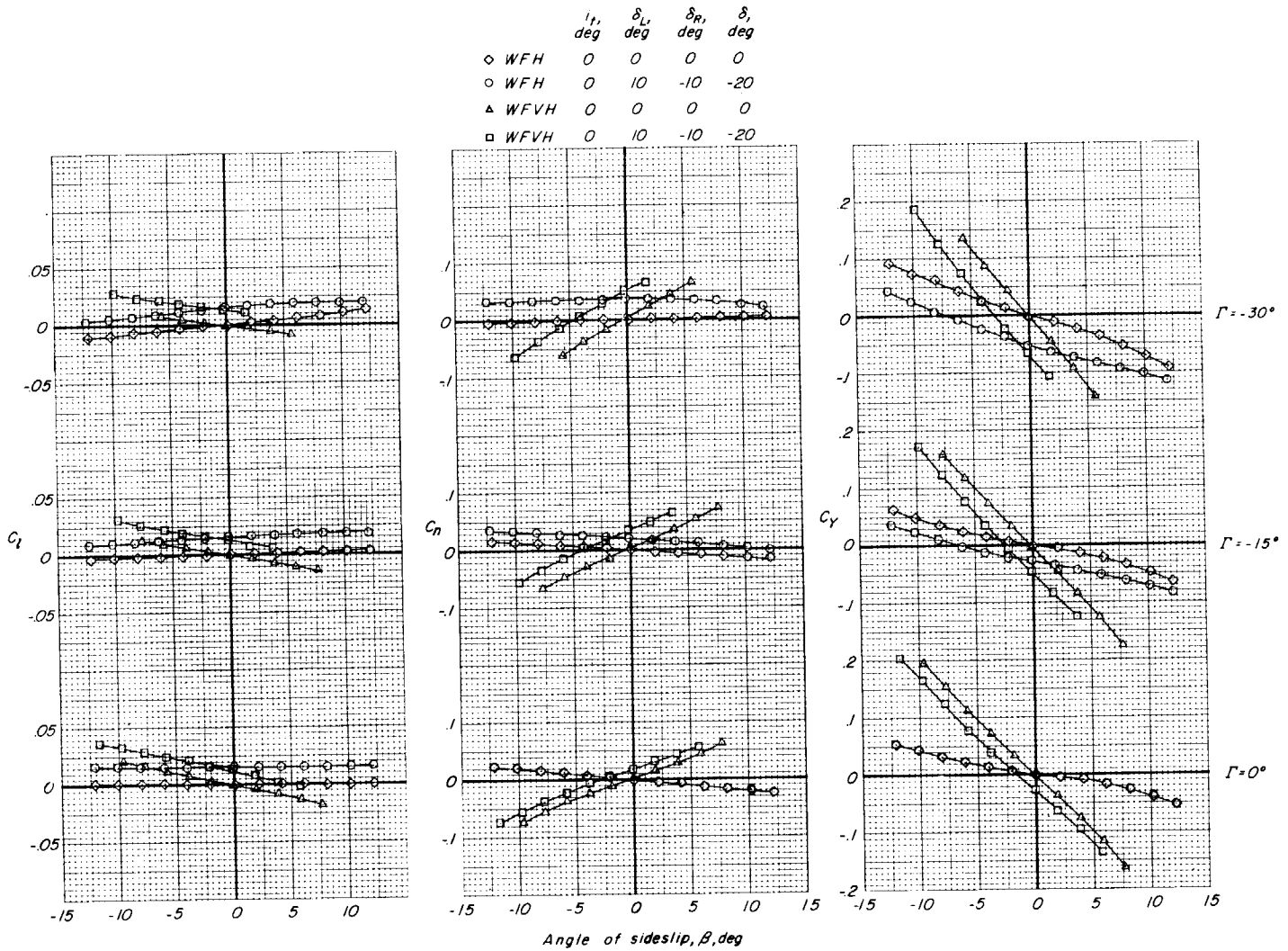

Figure 13.- Effect of sideslip on the lateral control characteristics of each tail dihedral angle with and without vertical tail at M = 0.80 and $\alpha = 0^{\circ}$.

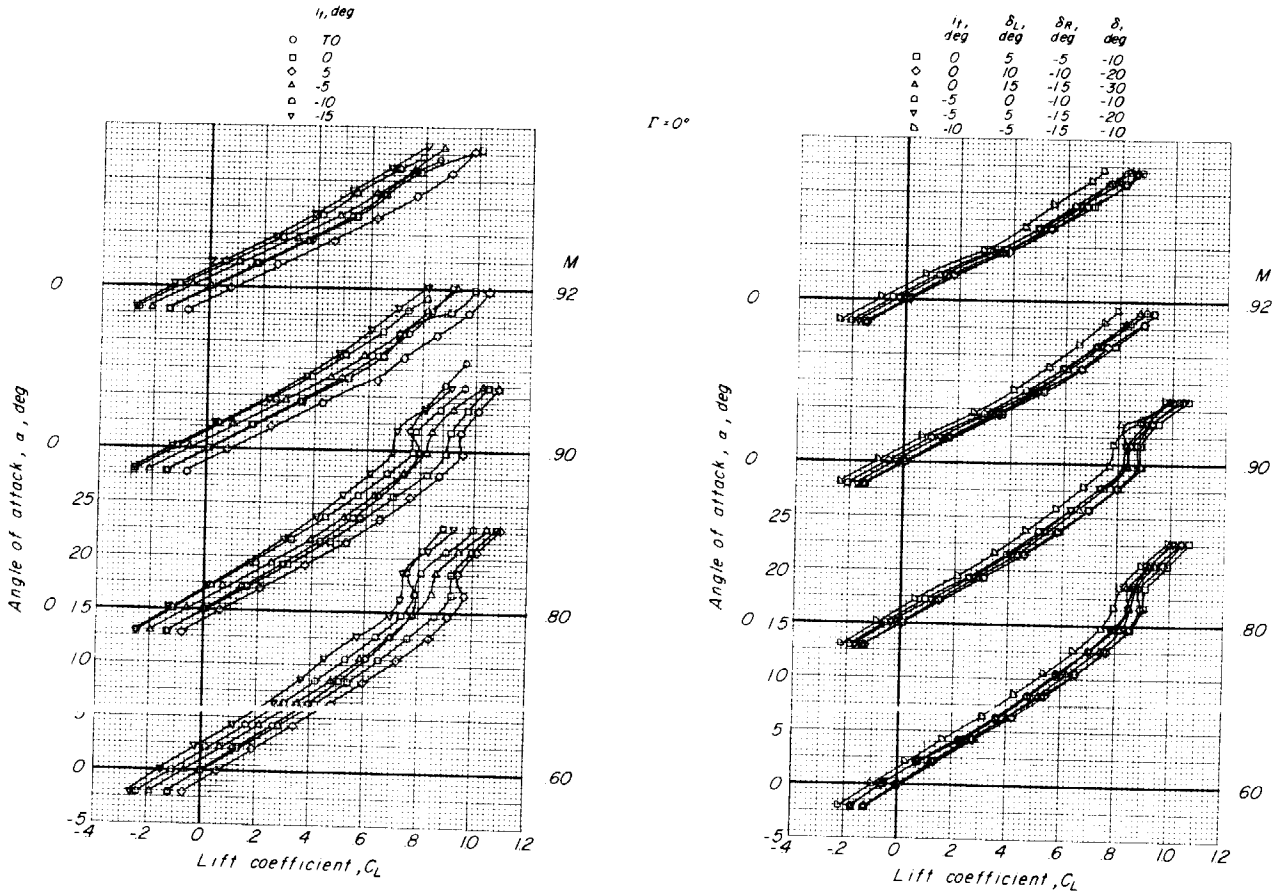

(a) Variation of α with C_L.

Figure 14.- Longitudinal aerodynamic characteristics of model having symmetrical and asymmetrical horizontal-tail deflection for $\Gamma = 0^\circ$.

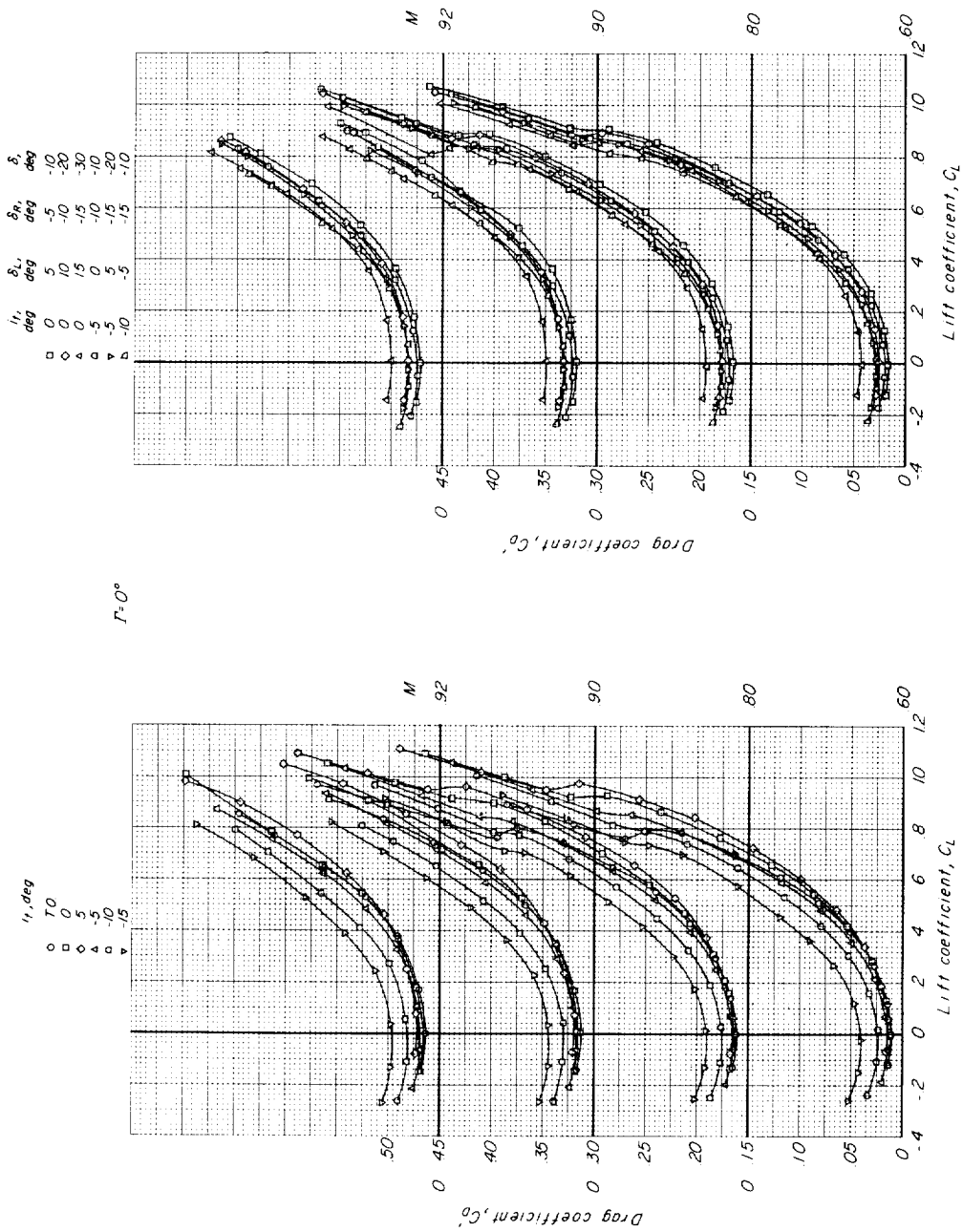

(b) Variation of C_D' with C_L.

Figure 14.- Continued.

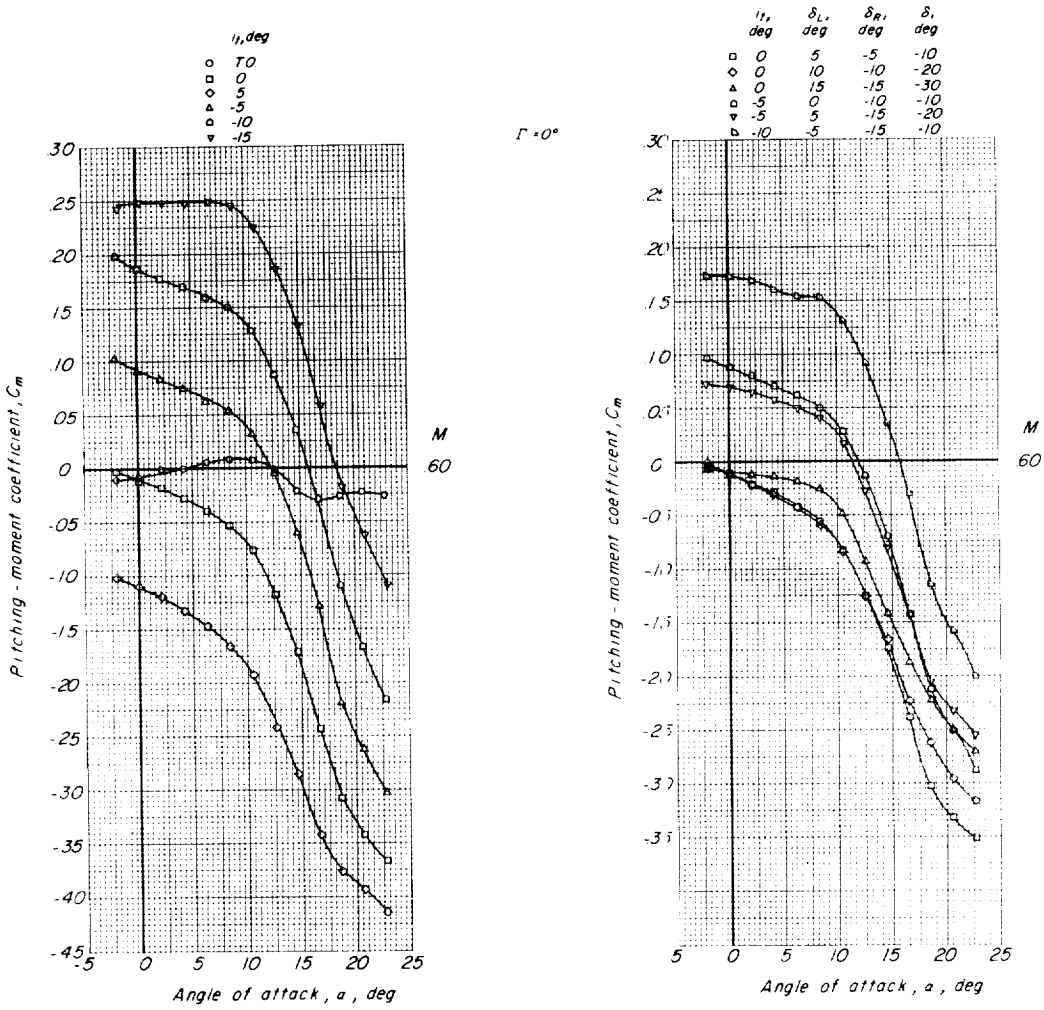

(c) Variation of C_m with α.

Figure 14.- Continued.

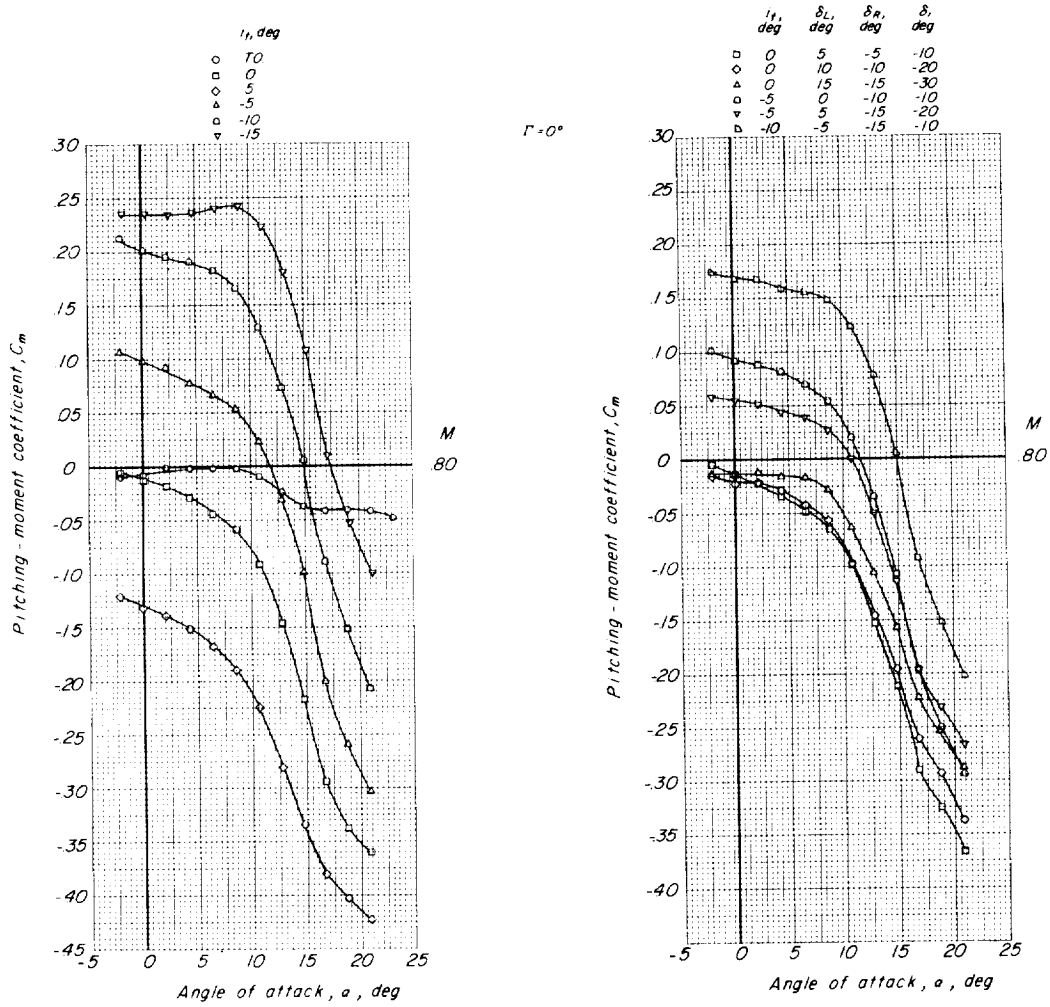

(c) Continued.

Figure 14.- Continued.

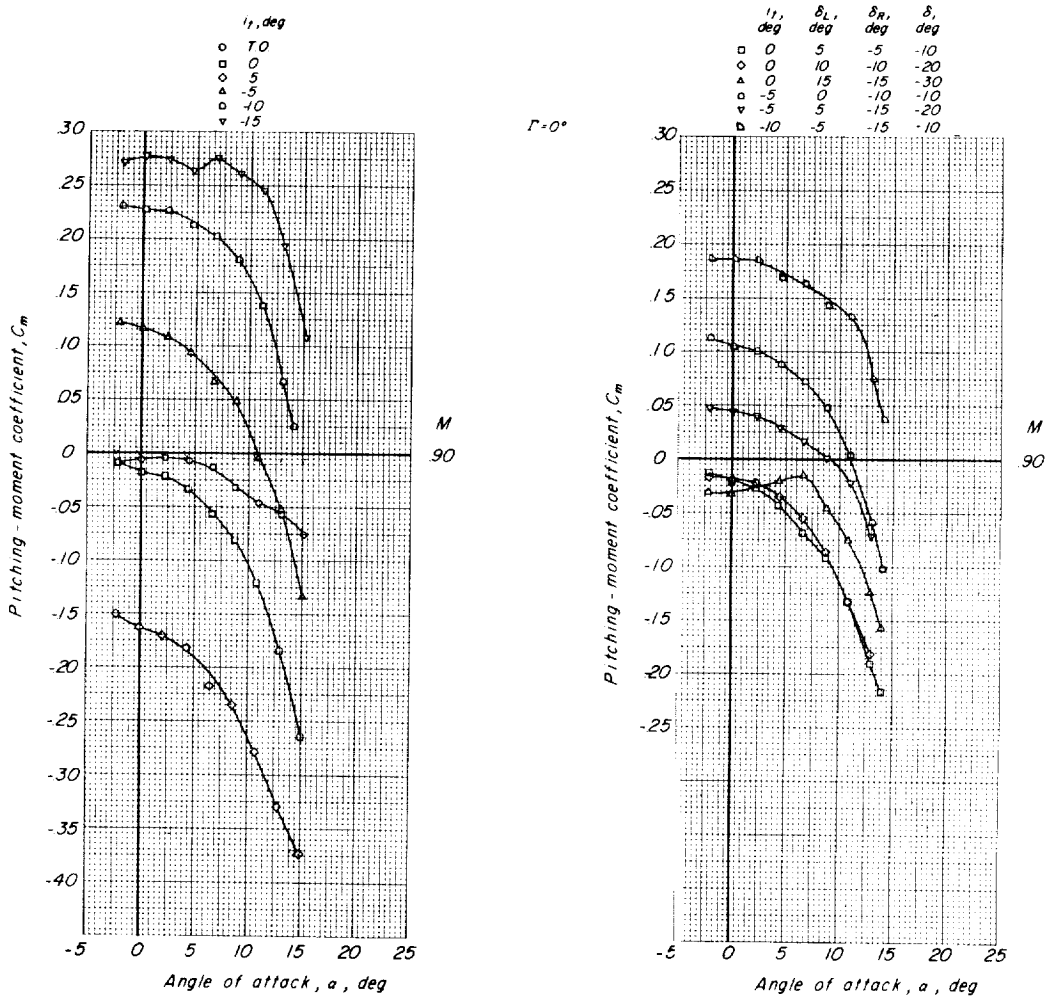

(c) Continued.

Figure 14.- Continued.

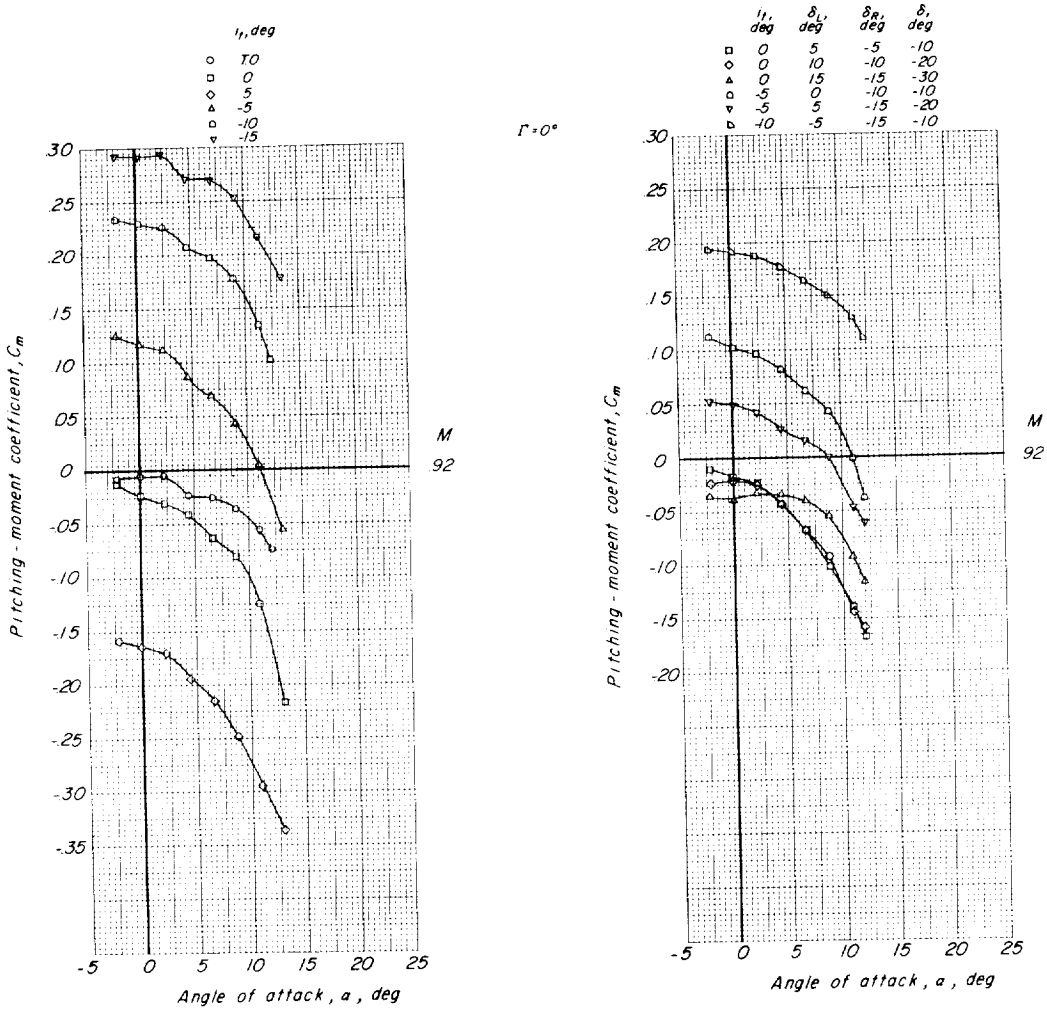

(c) Concluded.

Figure 14.- Concluded.

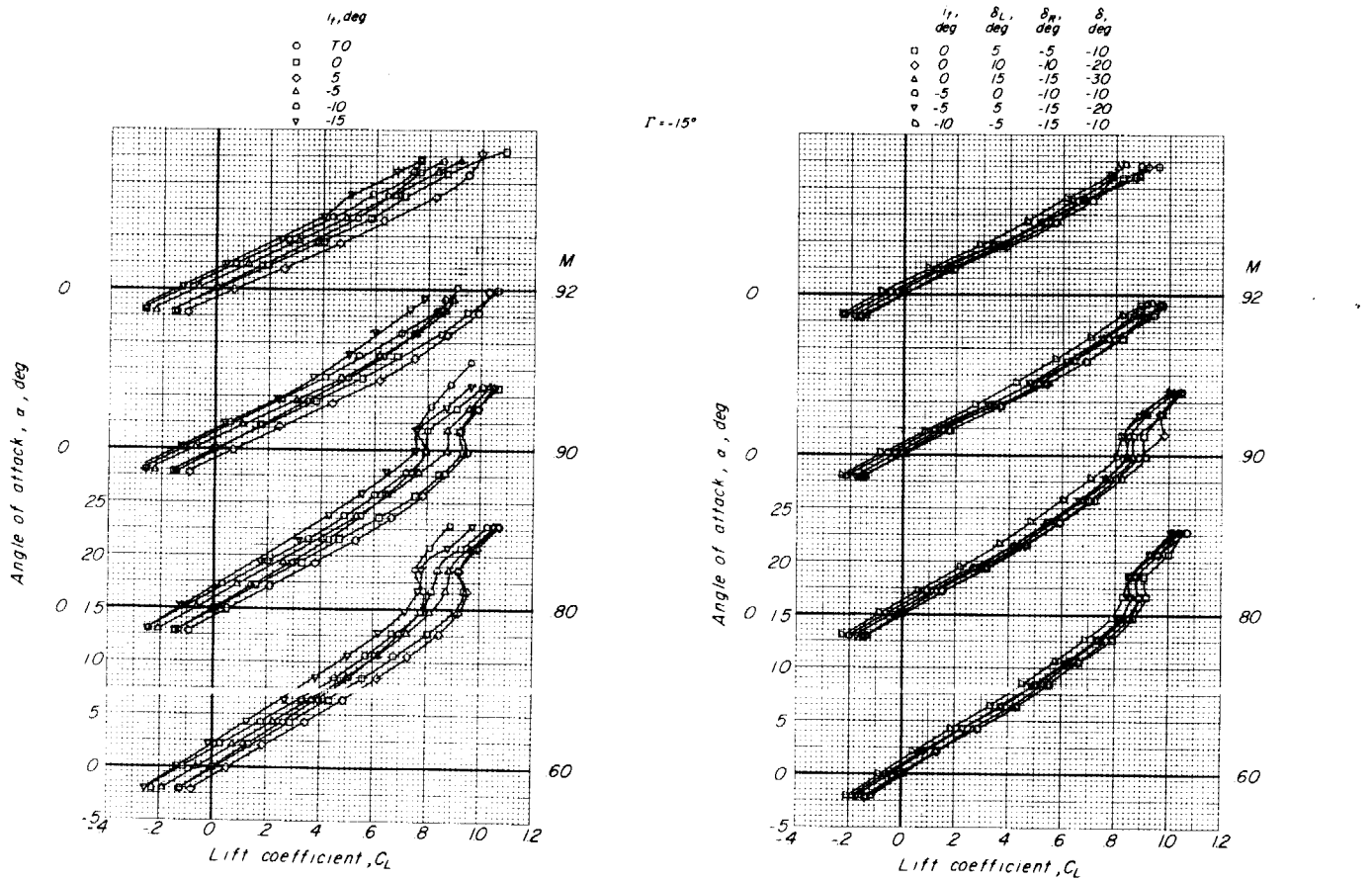

(a) Variation of α with C_L.

Figure 15.- Longitudinal aerodynamic characteristics of model having symmetrical and asymmetrical horizontal-tail deflections for $\Gamma = -15^\circ$.

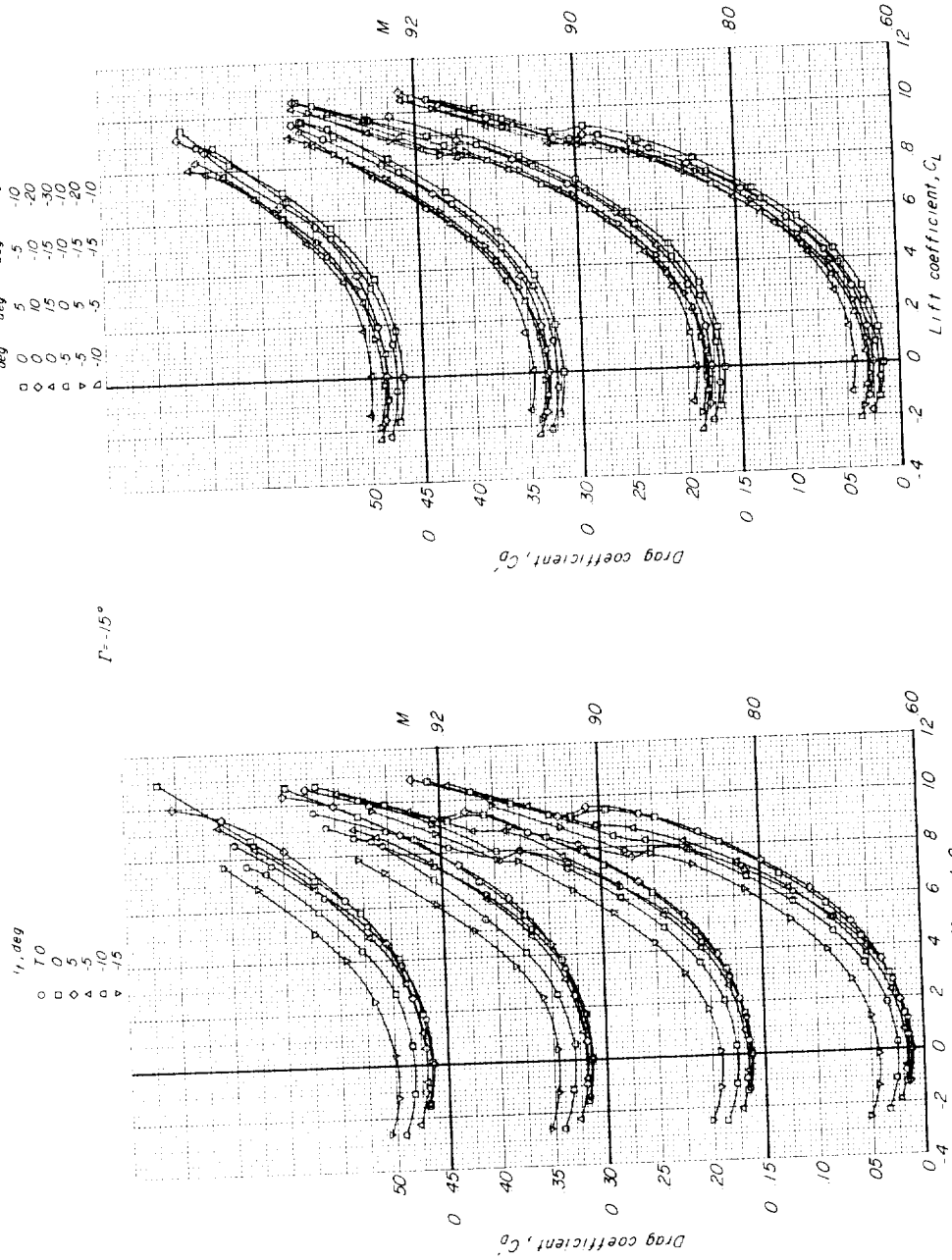

(b) Variation of $C_{D'}$ with C_L.

Figure 15.- Continued.

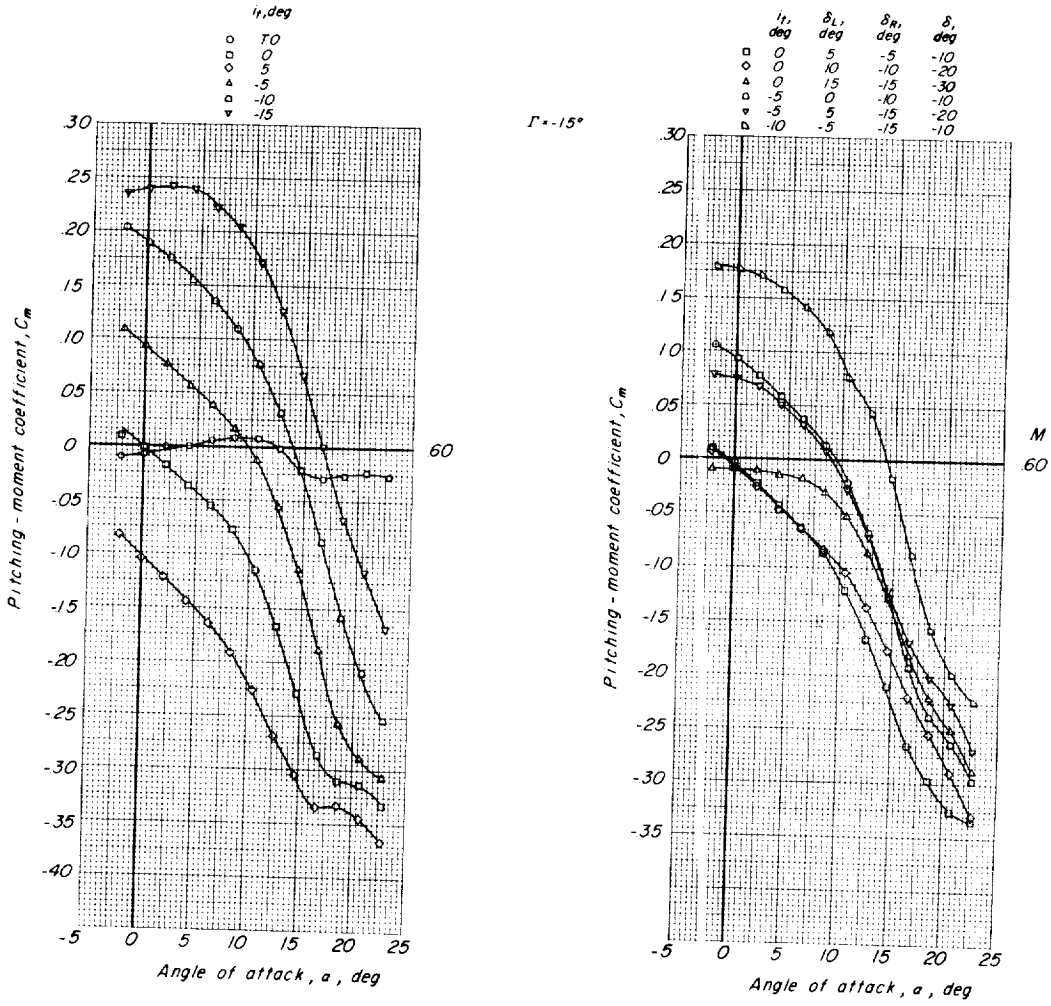

(c) Variation of C_m with α.

Figure 15.- Continued.

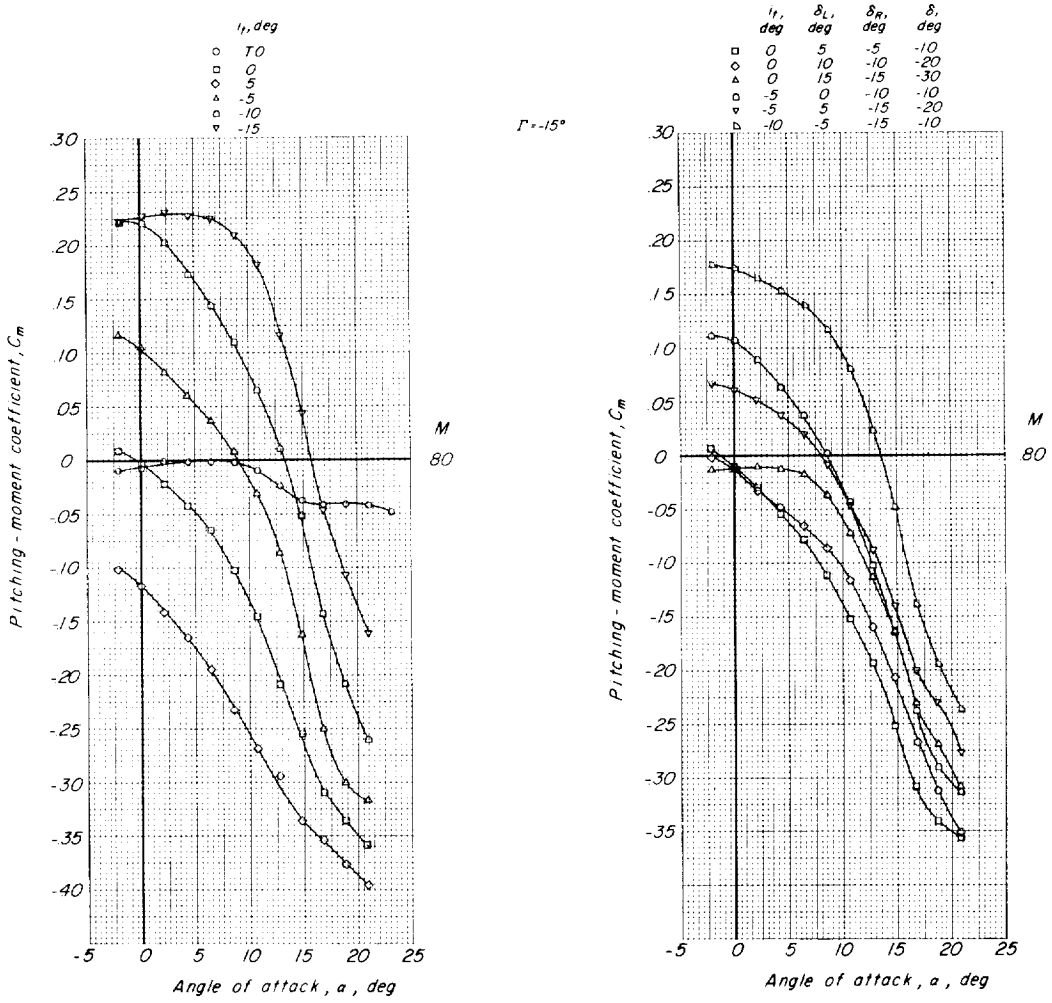

(c) Continued.

Figure 15.- Continued.

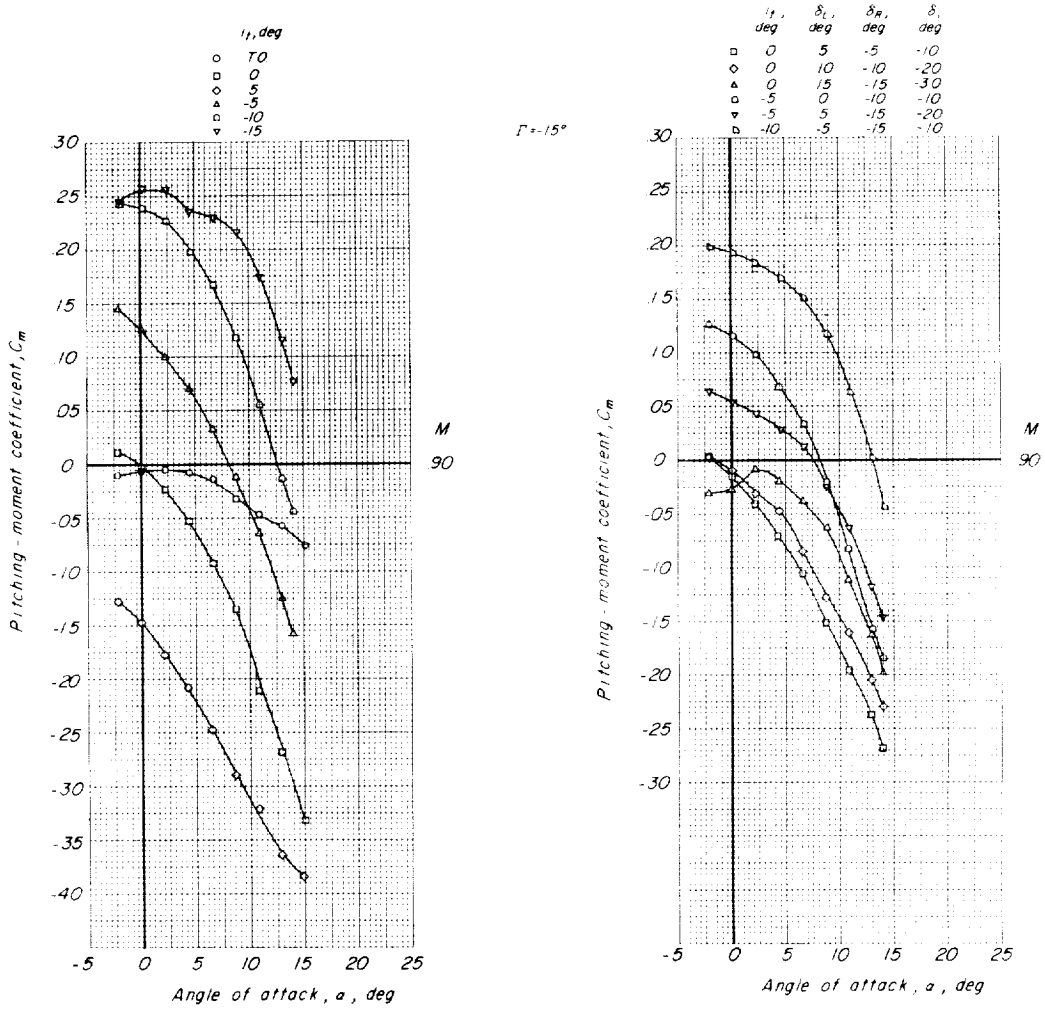

(c) Continued.

Figure 15.- Continued.

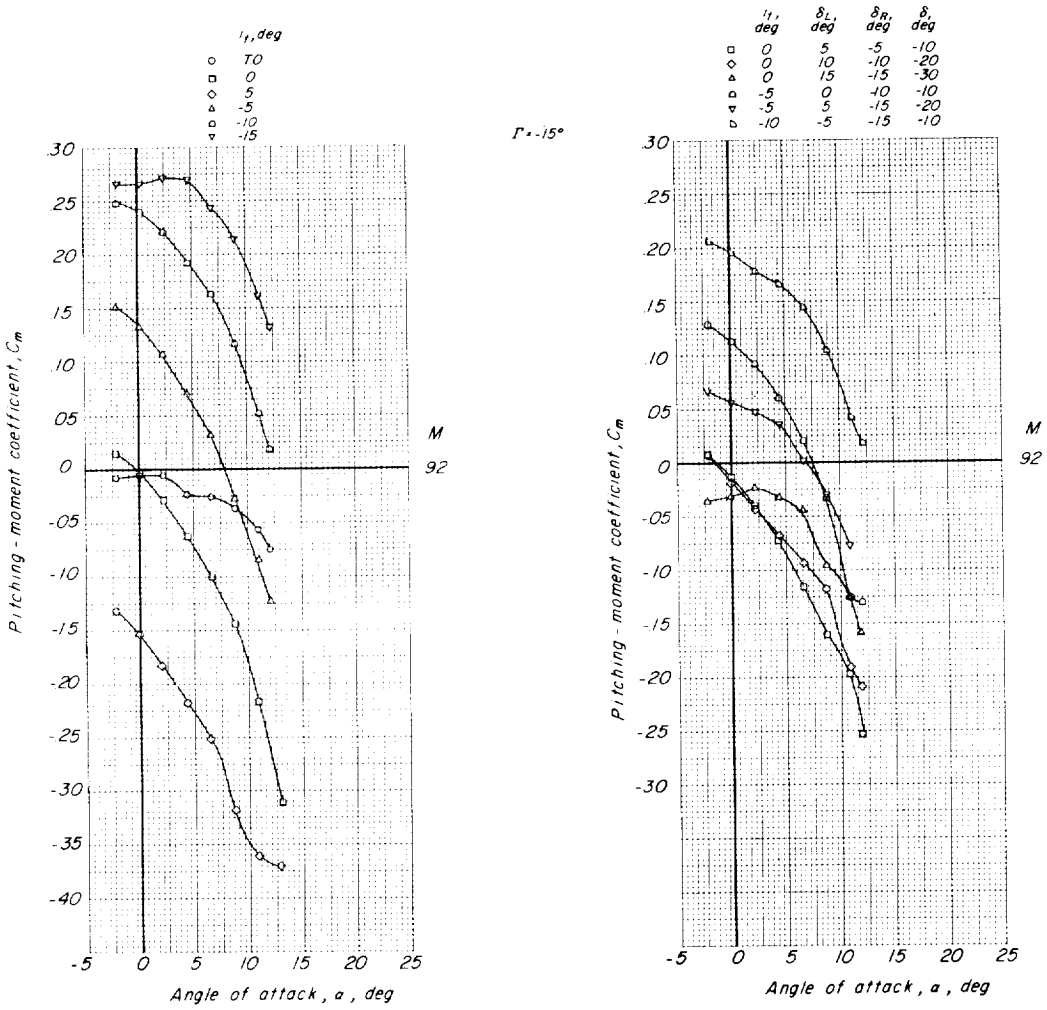

(c) Concluded.

Figure 15.- Concluded.

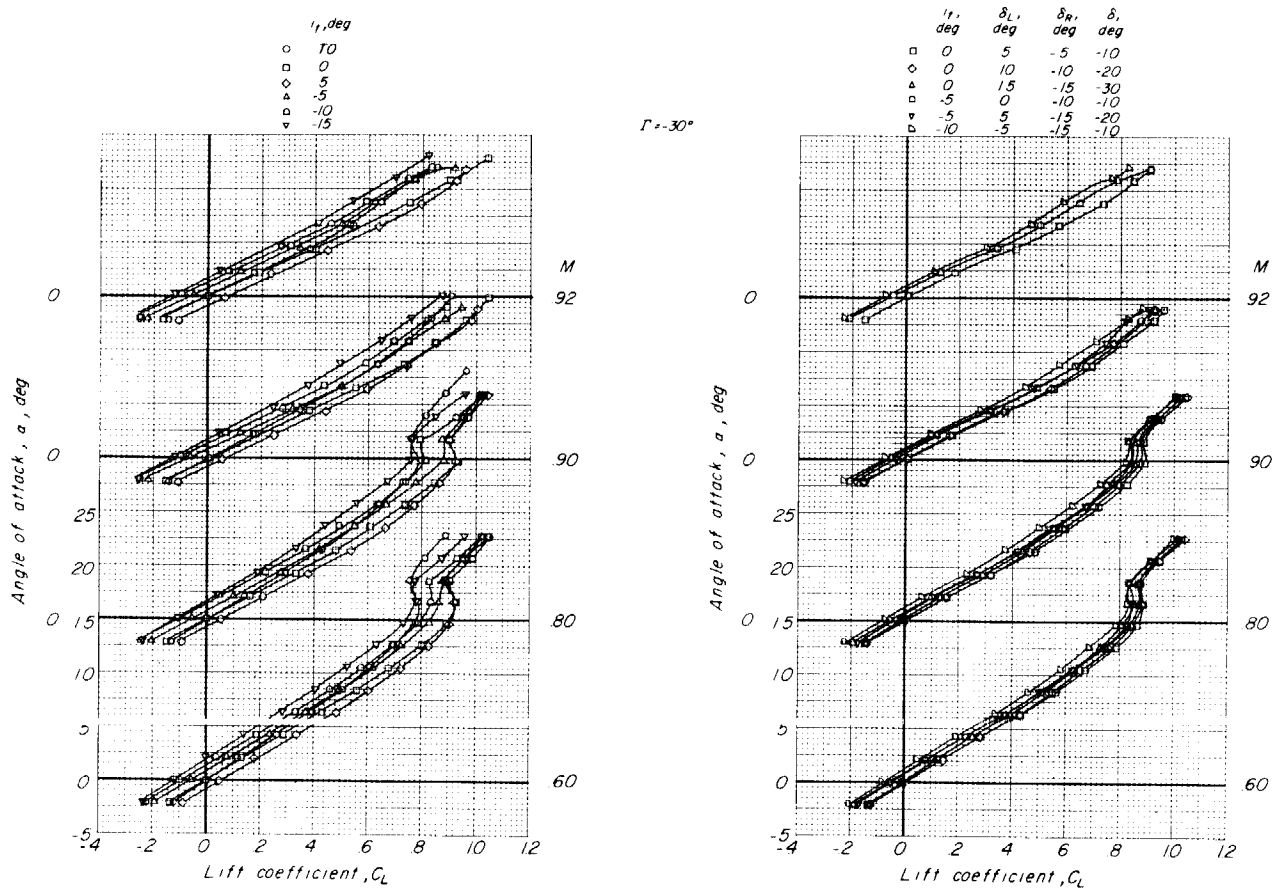

(a) Variation of α with C_L.

Figure 16.- Longitudinal aerodynamic characteristics of model having symmetrical and asymmetrical horizontal-tail deflections for $\Gamma = -30^\circ$.

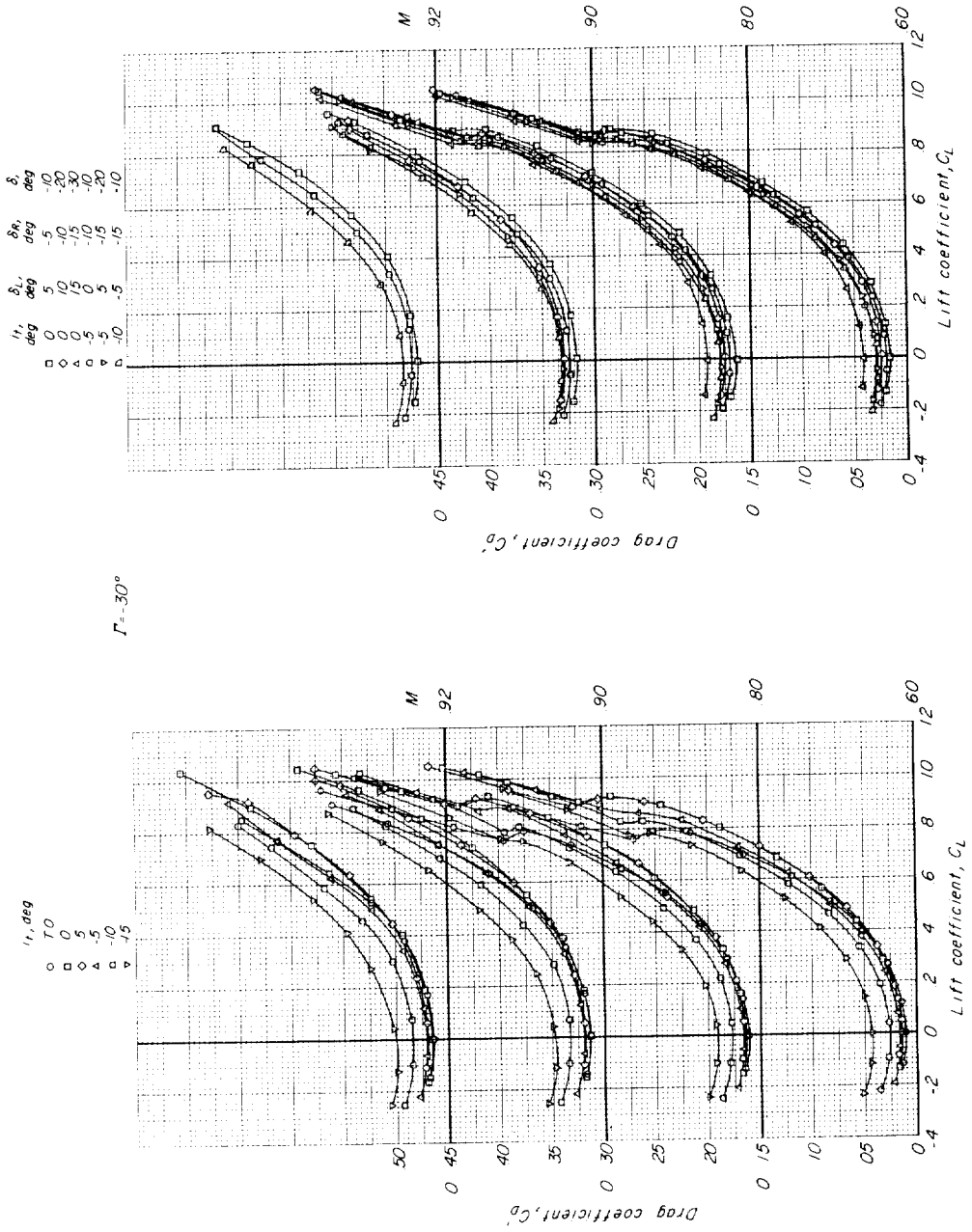

(b) Variation of C'_D with C_L.

Figure 16.- Continued.

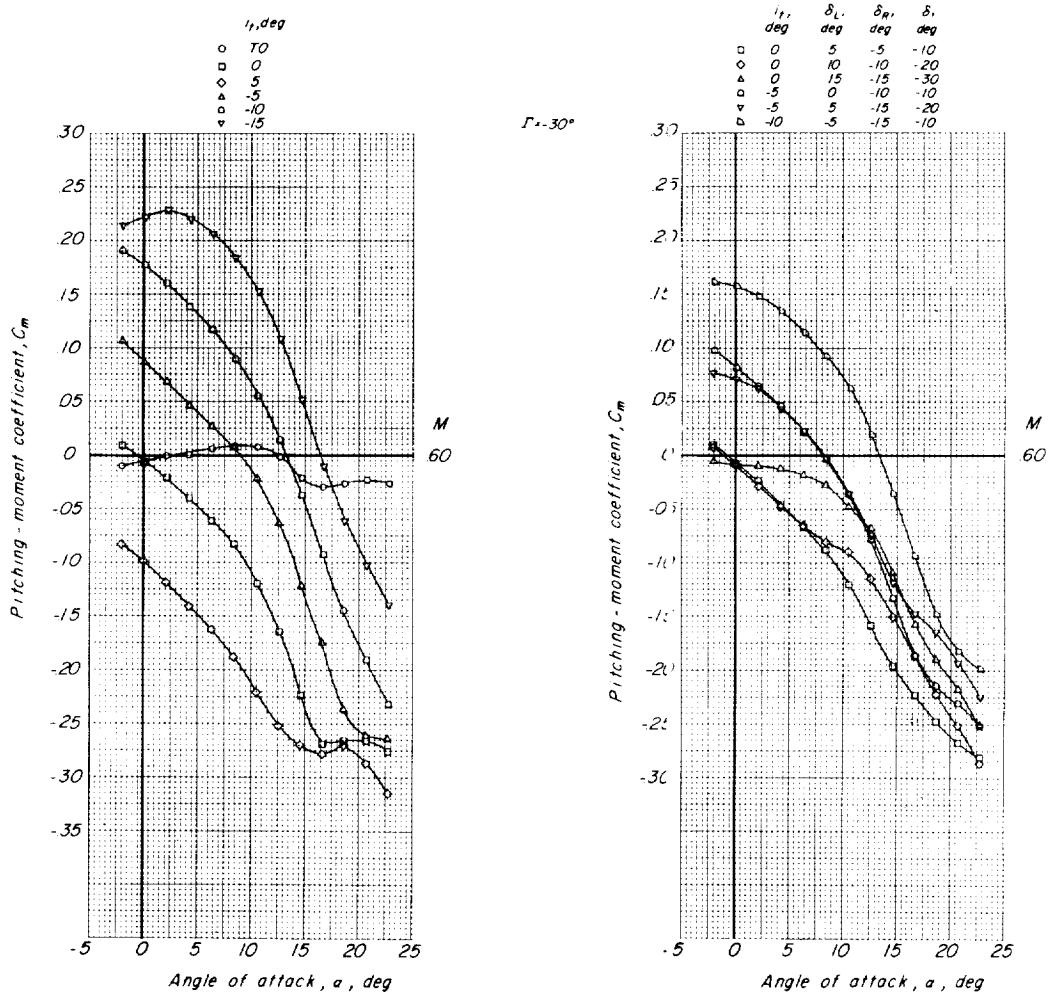

(c) Variation of C_m with α.

Figure 16.- Contirued.

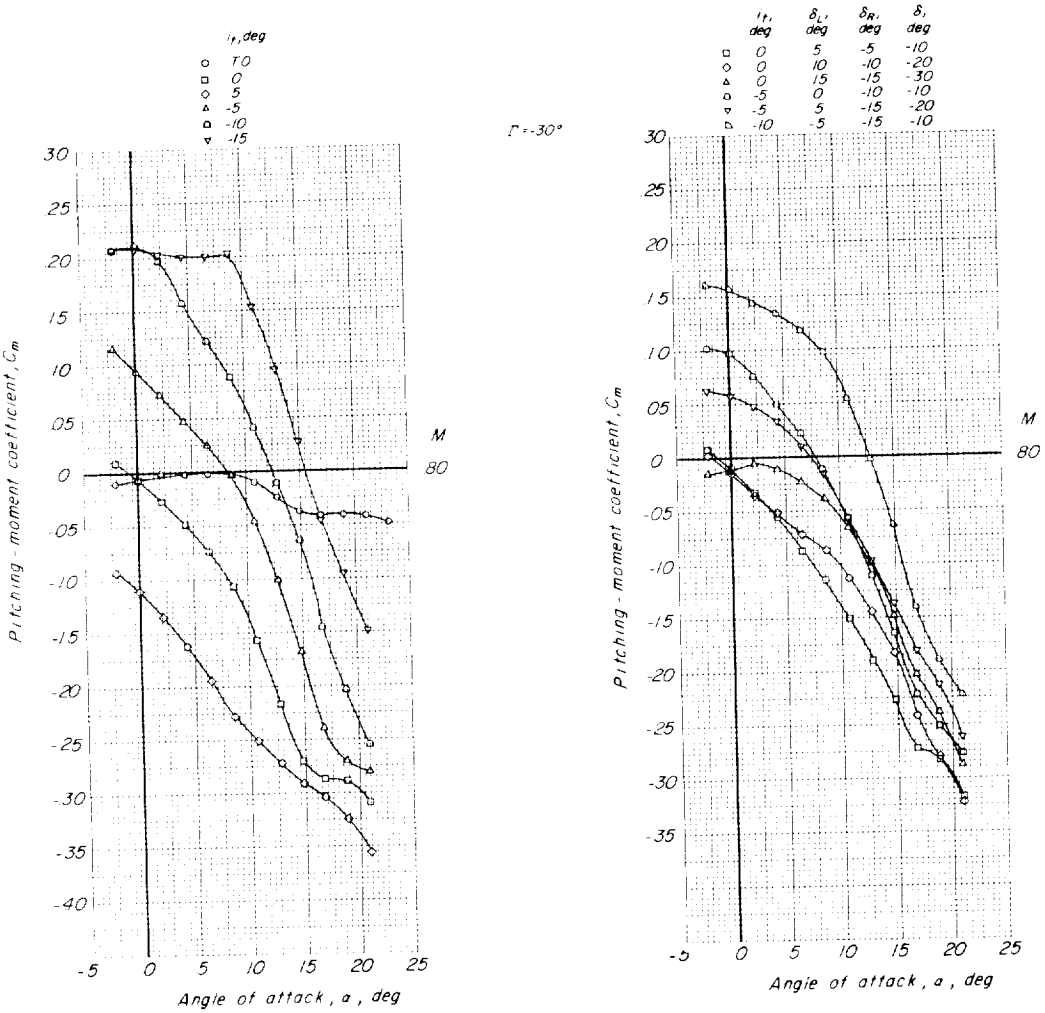

(c) Continued.

Figure 16.- Continued.

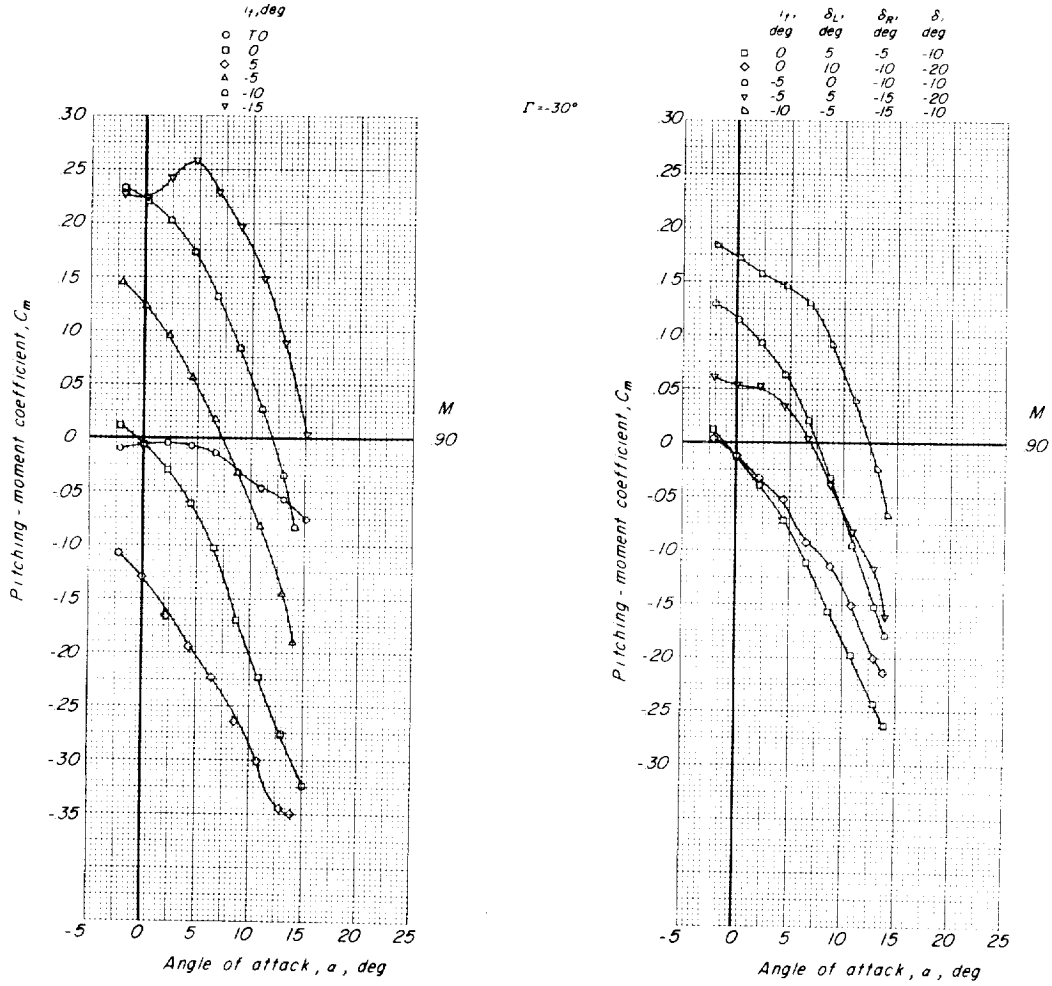

(c) Continued.

Figure 16.- Continued.

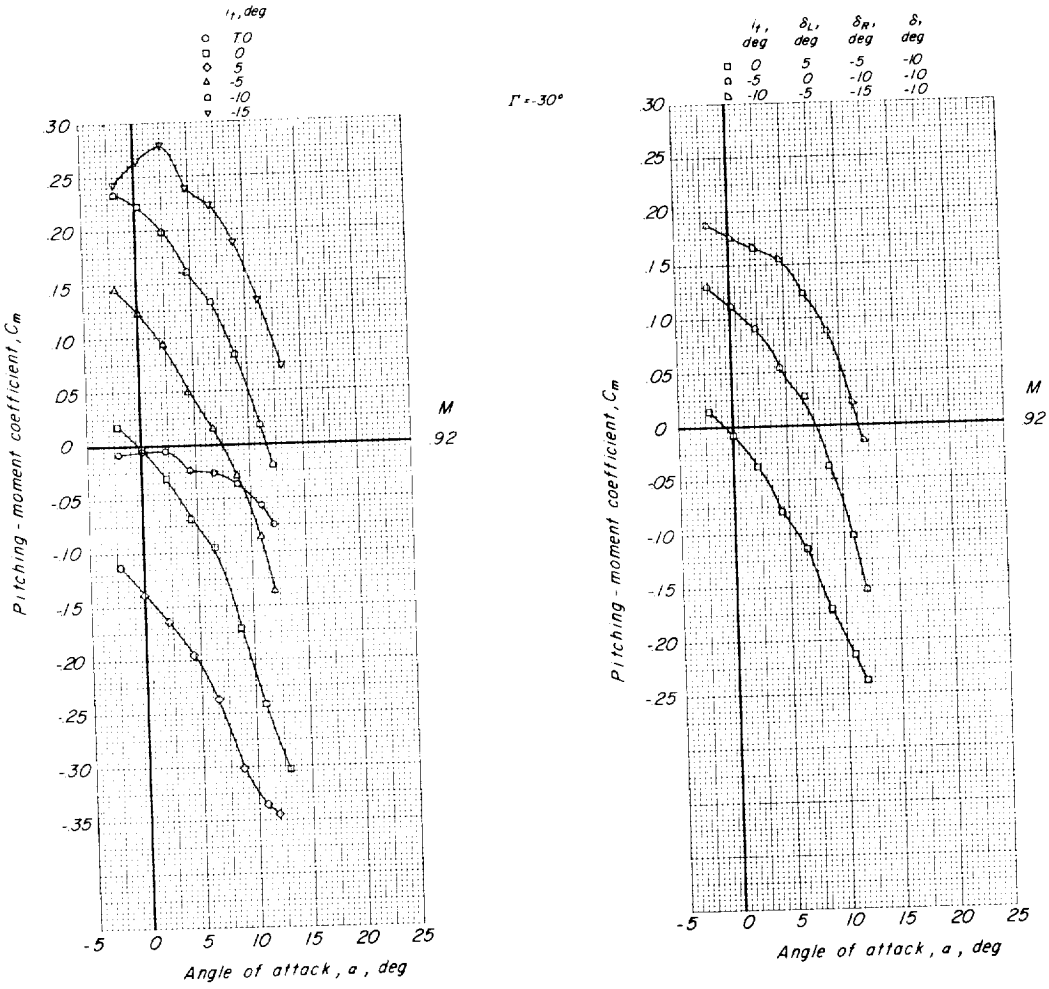

(c) Concluded.

Figure 16.- Concluded.

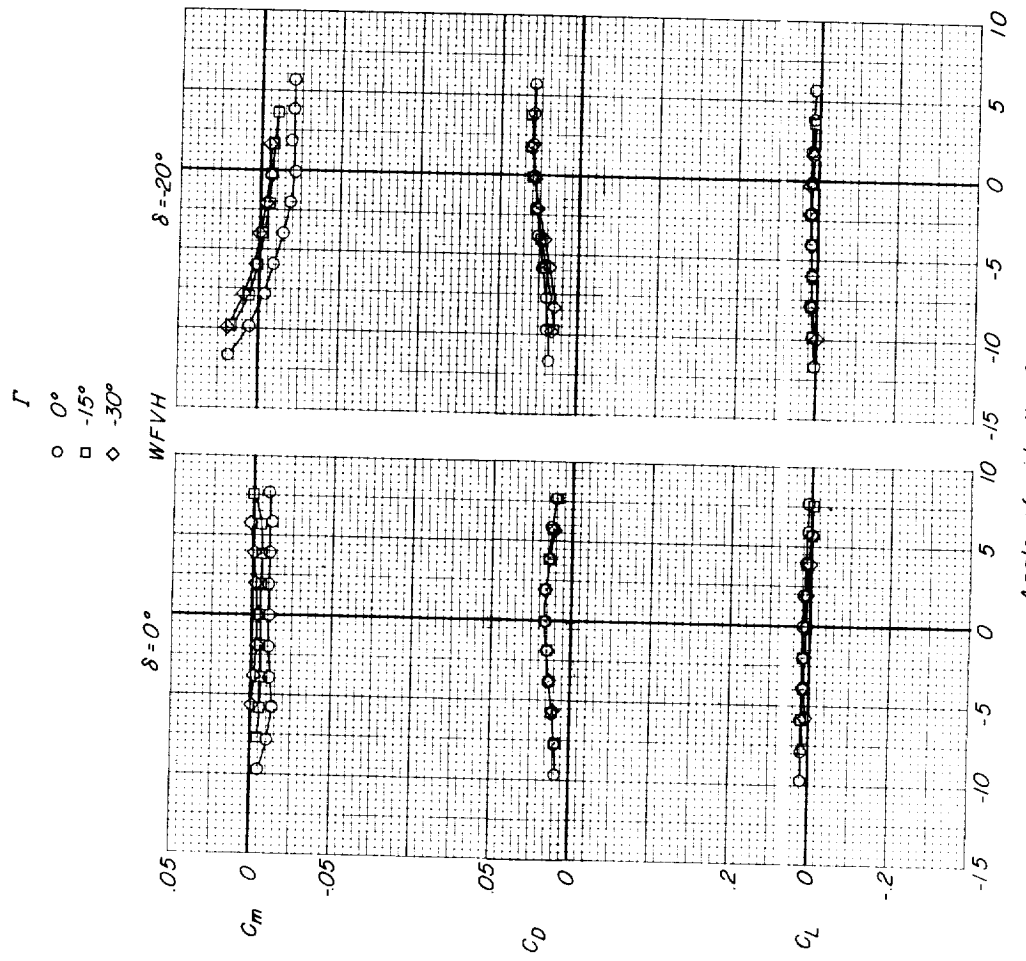

Figure 17.- The effect of sideslip on the longitudinal aerodynamic characteristics of the complete-model configuration at M = 0.80 and effective stabilizer setting of zero.